Prefrontal coding of learned and inferred knowledge during REM & NREM sleep

Authors

Kareem Abdou[1,2,3,4], Mohamed H. Aly[1,2,4,5], Ahmed Z. Ibrahim[1,2,3,4], Kiriko Choko[1,2,4], Masanori Nomoto[1,2,4], Reiko Okubo-Suzuki[1,2,4], Shin-ichi Muramatsu[6,7], Kaoru Inokuchi[1,2,4*]

Affiliations

[1]Research Centre for Idling Brain Science, University of Toyama, Toyama, 930-0194, Japan

[2]Department of Biochemistry, Graduate School of Medicine and Pharmaceutical Sciences, University of Toyama, Toyama, Japan

[3]Department of Biochemistry, Faculty of Pharmacy, Cairo University, Cairo 11562, Egypt

[4]CREST, Japan Science and Technology Agency (JST), University of Toyama, Toyama, Japan

[5]Pharmacology Department, Faculty of Pharmacy, The British University in Egypt, Cairo 11837, Egypt

[6]Division of Neurological Gene Therapy, Centre for Open Innovation, Jichi Medical University, Tochigi 3290498, Japan

[7]Centre for Gene and Cell Therapy, The Institute of Medical Science, The University of Tokyo, Tokyo 1088639, Japan

[*]Correspondence should be addressed to K.I.: inokuchi@med.u-toyama.ac.jp

ABSTRACT

Idling brain activity has been proposed to facilitate inference, insight, and innovative problem-solving[1-4]. However, it remains unclear how and when the subconscious brain can create novel ideas. Here, we show coordinated roles of non-rapid eye movement (NREM) and rapid-eye movement (REM) sleep in weaving inferential information from learned information. In a transitive inference paradigm, mice gained the inference one day, but not shortly, after complete training. Inhibiting the neuronal computations in the anterior cingulate cortex (ACC) during post-learning either NREM or REM sleep, but not wakefulness, disrupted the inference without affecting the learned knowledge. *In vivo* Ca^{2+} imaging showed gradual development of inference-related representation, peaking at post-training REM sleep. Neurons representing learned information co-reactivated significantly during post-training NREM sleep, while their co-reactivation with neurons representing inferential information was significantly higher during REM sleep. Furthermore, after insufficient learning, artificial activation of medial entorhinal cortex-ACC dialogue during only REM sleep created inferential knowledge. These findings suggest that NREM sleep organizes the scattered learned knowledge in a complete hierarchy, while REM sleep computes the inferential information from the organized hierarchy. Collectively, our study provides a mechanistic insight on NREM and REM coordination in weaving inferential knowledge, thus highlighting the power of idling brain in cognitive flexibility.

Introduction

Cognitive flexibility is a distinctive feature that is required for higher learning[5]. Inferential reasoning is a prominent property of cognitive flexibility since it relies on flexible and systematic organization of existing knowledge[3,5]. Activation patterns of neurons in the medial prefrontal cortex (mPFC) have been suggested to represent inferential reasoning[6,7].

Experience-related neural representations are re-expressed during post-learning awake rest and sleep periods[8,9]. This neural replay has been proposed to consolidate memories[8,10-13]. Previous work has found that awake replay events that occur during a spatial task not only represent recent experiences, but also novel spatial paths that might be confronted, which indicates that a whole spatial map has been formed[14-16]. Targeted reactivation of an implicitly learned sequence memory during sleep enables the development of explicit awareness of that sequence[17]. Previous reports have shown an offline improvement in a word-pair association task following sleep[18-21].

Enhanced cognitive performance has been linked with offline activity during non-rapid eye movement (NREM)[22] and rapid eye movement (REM)[23] sleep, but the most pertinent sleep stage and the circuits involved are still unclear. REM and NREM sleep have unique neurophysiological processes that impact cognition[24,25]. REM sleep is characterized by ponto-geniculo-occipital waves, theta rhythm, high acetylcholine levels, and upregulation of plasticity-related genes[26]. Long-term potentiation is easily induced during REM sleep[27]. NREM sleep is characterized by regular occurrence of slow wave delta activity, high protein synthesis levels, and a rise in depotentiation-related genes and drop in long-term potentiation-related genes[24,28-33]. Therefore, sleep stages differentially affect neuronal functions and may therefore modify cognitive capabilities. Furthermore, previous reports have proposed that NREM and REM sleep have differential contribution in several brain functions; for example, memory consolidation[34], visual learning[35], skills and schemas[36]. Consequently, we hypothesize

that NREM and REM sleep have distinct roles in the processing of learned and inferential information.

The aforementioned studies[14-17,22,23] highlight the involvement of online and offline brain activity in cognitive flexibility. However, the temporal, cellular and circuit mechanisms underlying the emergence of inference from chronologically separated, yet overlapping, experiences are still unclear.

Results

Randomizing existing knowledge is necessary for the emergence of inferential behaviour

We developed a transitive inference paradigm in mice that assesses the ability to infer new information that was not learned before, based on previous knowledge of overlapping memories. First, food-restricted mice were allowed to explore and habituate to an arena consisting of five different contexts (Context A, B, C, D, and E) (Fig. 1a). These contexts were different in terms of geometry and/or floor texture and/or wall color and pattern. During the habituation period, mice did not show a significant innate preference to any context (Extended Data Fig. 1). Then, they were trained on a series of two-context discrimination trials called premise pairs (A > B, B > C, C > D, and D > E; where “>” means that the former context is more preferred than the latter one). Mice should prefer the context in which they were rewarded with a sucrose tablet. Every day, mice were trained on two premise pairs in two sessions, with each session consisting of five trials. During each trial, mice were put into the arena with only two opened contexts, while the other three contexts were closed (Fig. 1b). After staying in the assigned context for a consecutive 10 sec, mice received a sucrose tablet (Extended Data Video 1). After reaching the criterion for correct performance (80% correct trials) in the four premise pairs (Fig. 1c), mice were divided into two groups. The first group was subjected to reinforcement sessions only, while the second group received randomized training sessions in

which each pair was presented with a different pair every day (Fig. 1b and Methods). Then, mice were subjected to inference (B & D) and non-inference (A & E) tests on the last day of training (T1) and in the subsequent 3 days (T2, T3, and T4). Contexts B and D had an equal valence during training as they were the preferred context in one premise pair (B > C and D > E, respectively), and were the avoided context in the other premise pair (A > B and C > D, respectively), such that the performance in the inference test would be purely due to inference from the hierarchy. On the other hand, context A was usually the preferred context, while context E was usually un-preferred; therefore, the performance during tests with the A and E contexts would not be due to the inference. Mice that received randomized training inferred correctly in all tests except for in T1, as shown by an increased number of correct trials and a decreased latency time to choose the correct context (Fig. 1d, e). On the other hand, mice that received reinforcement training only without randomization did not exhibit inference in any tests (Fig. 1d, e); however, they had successfully learnt the original premise pairs (Fig. 1c), which indicates that knowledge of the premise pairs did not assure the emergence of inference. This showed the necessity of randomization during acquisition of the premise pairs knowledge for gaining the inference. In both groups, the percent of correct trials was significantly higher than chance level (50%) in the non-inference test, and their memories of the original premises were intact (Extended Data Fig. 2a).

The emergence of inference requires sleep after training

The inability to infer correctly in T1 and the expression of inference in T2 suggest that inference does not arise online during the repeated training, but instead may require an incubation period or sleep following training. To examine which factor is critical for the inference process, we kept the incubation period intact (the same as before), but mice were sleep-deprived for 4 h directly after test sessions (Fig. 1f). Mice met the criterion for correct training performance,

with a non-significant difference in the percent of correct trials across all premise pairs (Fig. 1g). Sleep deprivation blocked the inference; the correct performance of mice remained at chance level and their decision making was delayed (Fig. 1h, i). However, sleep deprivation did not affect performance on the non-inference test or the original premises' tests (Extended Data Fig. 2b). This suggests that sleep after the last training is crucial for constructing the whole hierarchy of preferences and the subsequent development of inference, but that it is not essential for the A and E pair or for the maintenance of the original premises' representations. The inferential behaviour that appeared in T2 in the inference group was not due to learning during T1 since mice were not provided with sucrose in T1, even when the correct choice was made.

To test whether the inference observed in T2 was facilitated by T1 exposure in which B and D pair was presented to mice, mice were exposed to the same behaviour protocol without exposure to T1 (Extended Data Fig. 3a). After successful training phase (Extended Data Fig. 3b), mice inferred correctly during subsequent test sessions (Extended Data Fig. 3c, d). This result indicates that T1 exposure is not necessary for the emergence of inference during T2, which supports that inference is a higher-order process than a result of direct learning.

Organizing existing knowledge into a hierarchical order is necessary for inference

To confirm that mice gained the inference after arranging the premise pairs into a hierarchical order, we trained a group of mice in the same arena, with the same number of trials, but with premise pairs that did not form a complete hierarchy (A > B, B > C, E > D, D > C; Extended Data Fig. 4a, b). Mice learnt the premise pairs well and reached the criterion of correct performance (Extended Data Fig. 4c). Lacking the complete hierarchy led to failed inference (Extended Data Fig. 4d, e), although mice memorized the original premise pairs well (Extended Data Fig. 4g). Since context A and context E were always preferred in the premise pairs training,

143 mice did not prefer either of these during the non-inference test (Extended Data Fig. 4f). These
144 results demonstrate that extracting inference requires the organization of previously acquired
145 knowledge into a hierarchical order.
146

147 **Prelimbic cortex activity is not required for the emergence of inference**

148 The mPFC has been proposed to process the mental schema that is utilized to build an inference,
149 and may also compute the inferred outcomes[6,7,37-39]. However, these proposals were derived
150 from lesion and functional brain imaging studies, and lack the causality for temporal and
151 topographic specificity that are necessary for inference development. To directly unravel these
152 ambiguities, we manipulated the activity of mPFC sub-region, the prelimbic cortex (PL) during
153 sleep and awake states. The PL of mice was injected with adeno-associated virus 9 (AAV9)
154 encoding a light-sensitive neuronal silencer (ArchT 3.0) with enhanced yellow fluorescent
155 protein under the control of calcium/calmodulin-dependent protein kinase II (CaMKII) to label
156 excitatory neurons with ArchT 3.0 (Extended Data Fig. 5a). Then, mice were subjected to the
157 transitive inference task, where optogenetic inhibition was performed during either
158 wakefulness or sleep on the last training day and testing days (Extended Data Fig. 5a, b). Mice
159 achieved the standard for correct performance in all premise pairs (Extended Data Fig. 5c, d).
160 Inhibiting PL activity during sleep or wakefulness after the training did not affect the inference,
161 non-inference test, or premise pairs memories (Extended Data Fig. 5e-h), which indicates that
162 PL activities during sleep and awake states are not required for the formation of inference.
163

164 **Anterior cingulate cortex computations during sleep are crucial for the emergence of**
165 **inference**

166 Next, we manipulated another mPFC sub-region, the anterior cingulate cortex (ACC). Mice
167 received injections into the ACC of AAV-CaMKII-ArchT 3.0-eYFP to label excitatory neurons

168 with ArchT 3.0 (Fig. 2a). Afterwards, mice completed the transitive inference task, where
169 optogenetic inhibition was performed during either wakefulness, NREM sleep, or REM sleep
170 on the last training day and testing days (Fig. 2b, c). Mice learnt the premise pairs well, which
171 was reflected by the high number of correct trials that reached the criterion for correct
172 performance (Fig. 2d). Optogenetic inhibition of the ACC (Extended Data Fig. 6a) during
173 wakefulness did not impact inference ability, as mice achieved a high correct performance
174 during inference, non-inference, and premise pairs tests (Fig. 2e, f and Extended Data Fig. 2c).
175 Conversely, mice that received optogenetic inhibition of the ACC either during NREM or REM
176 sleep failed to infer correctly, and the percent of correct trials was not significantly different
177 from chance level (Fig. 2e). Moreover, the latency to choose was significantly longer in the
178 NREM and REM groups than that of the awake group (Fig. 2f). These data indicate that ACC
179 computations are necessary for the evolution of inference ability during sleep, but not during
180 wakefulness. However, this perturbation to ACC dynamics had no influence on the non-
181 inference pairs or the maintenance of premises knowledge (Extended Data Fig. 2c).
182

183 **Inference representations develop gradually, peaking during REM sleep after training**

184 To examine how the offline brain organizes the previously acquired knowledge and
185 builds novel inferential information, we tracked the ACC neuronal activity via Ca2+ imaging.
186 Wildtype mice were injected with AAV9-Syn-janelia-GCaMP7 into the ACC (Fig. 3a) and a
187 custom-built electroencephalogram/electromyography (EEG/EMG) 5-pin system was installed
188 into the skull, as previously described[40], to record the neuronal dynamics during awake and
189 sleep states (Fig. 3b). The same ACC neurons were tracked across sessions[8] along the transitive
190 inference task (Fig. 3c-e), using an automated sorting system[41] to extract each neuron's calcium
191 (Ca2+) activity which were normalized to z-scores (see methods for details). Offline stages
192 either awake or sleep were differentiated according to the automatically enumerated EMG root

193 mean square value (ERMS), EEG delta power (1–4 Hz) RMS (dRMS), and EEG theta power
194 (6–9 Hz) RMS, as described previously[40,42]. Sleep stages discrimination was concluded based
195 on the delta/theta ratio value (Fig. 3b; see Methods for details).

196 Next, we employed combination of principal component and independent component
197 analyses (PCA/ICA) to identify the neuronal assembly patterns and track their activity over
198 time (Fig. 3f). We isolated different synchronized patterns during T2 session (Inference
199 session) and tracked them over time. After that, we identified the inference-related patterns
200 according to 3 criteria. First, they appeared in both T2 and T3 sessions just before the correct
201 choice (entering and waiting in context B). Second, they appeared in T2 with an activation
202 strength significantly higher than their strength during T1 session where the inferential
203 behaviour was absent. Third, they did not appear during (B & C) and (C & D) sessions to
204 confirm that these patterns are not representing context B preference or context D avoidance.

205 Upon investigating the temporal emergence of inference-related patterns, we found that
206 they started to emerge from the randomization session and their activation strength increased
207 gradually, peaking at REM sleep after T1 session (Fig. 3g, i). Strength of inference-related
208 patterns was comparable between T2, T3 and REM 2 sessions, which was significantly higher
209 than their strength in the earlier sessions. This result indicates that significant inference
210 representations emerge during REM sleep after randomized training. Although inference-
211 related patterns appeared during T1 session, their strength were not high enough to trigger
212 inferential behaviour in T1. They were evident enough to elicit inferential behaviour in T2 and
213 T3 sessions, suggesting that the level of pattern strength predict the task performance.

214 On the other hand, we extracted neuronal patterns representing the premise pairs during
215 training sessions (see Methods). These patterns were divided into 3 groups; first, patterns
216 activated significantly during initial training than during randomized training, named initial
217 training-related patterns (Extended Data Fig. 7a). Second, patterns activated significantly

during randomized training than during initial training, named randomized training-related patterns (Extended Data Fig. 7b). Third, patterns activated significantly during both initial and randomized training than during the earlier sessions, named stable training-related patterns (Stable "Tr, Rand") (Fig. 3h). The stable "Tr, Rand" patterns representing both initial and randomized training were evident during REM sleep more than the initial training-related patterns, suggesting a higher contribution of stable "Tr, Rand" patterns in inference emergence (Extended Data Fig. 7c). Unlike inference-related patterns which reactivated during REM 2 more than NREM 2, stable "Tr, Rand" patterns reactivated similarly during NREM 2 and REM 2 sessions (Fig. 3h, i). Furthermore, comparing the activation strength of inference-related patterns and stable "Tr, Rand" patterns across sessions suggests that representations of learned and inferred information might be orthogonal (Fig. 3i).

Coactivity code underlies the emergence of inferential behaviour representation

Understanding ACC computations during NREM 2 & REM 2 sleep sessions would explain the mechanism underlying the transitional increase of activation strength of inference-related patterns between NREM 2 and REM 2 (Fig. 3g), which predicts the inferential behaviour. To address this aim, we assessed the co-activation index between different patterns by calculating the number of pairwise synchronized Ca2+ activities within 200 ms between neurons constituting each pattern (Fig. 4a, b). Neurons contributing to the stable "Tr, Rand" patterns were co-activated significantly higher during NREM 2 than during REM 2 and awake sessions, representing a significant interaction (Fig. 4c). Furthermore, neurons belonging to inference-related patterns interacted with those belonging to stable "Tr, Rand" patterns significantly higher during REM 2 than during NREM 2 and awake sessions (Fig. 4c).

To examine the contribution of each premise pair (A&B, B&C, C&D, D&E) to the coactivity code, we extracted the patterns uniquely representing each premise pair and tracked

243 the coactivity of their neurons. We counted the quadruple coactivation index between neurons
244 representing the 4 individual premise pairs and found that they coactivated together during
245 NREM 2 significantly more than during REM 2 session, which suggest organizing the learned
246 information in hierarchy during NREM sleep (Fig. 4d). When we counted the quintuple
247 coactivation index between neurons representing the 4 premise pairs and the inference patterns,
248 we found higher synchronized activity during REM 2 than NREM 2 (Fig. 4e).

249 These results indicate the complementary role played by NREM and REM sleep. The
250 learned knowledge is organized during NREM sleep, while it synchronizes with inferred
251 information during REM sleep that may increase the strength of inference-related patterns
252 leading to inferential behaviour. This two-step mechanism may explain the necessity of both
253 NREM and REM sleep for building cognitive inference. Moreover, neurons constituting
254 patterns of T1 session did not synchronize with those representing either training or inference
255 sessions (Fig. 4c), supporting that T1 session is not critical for the inferential behaviour
256 observed in T2 and T3.

257

258 **MEC→ACC crosstalk during REM sleep is sufficient to inspire inference from**
259 **inadequate training**

260 To establish a causal link between ACC coactivation code and inference processing,
261 we sought to identify and manipulate a neural circuit that is involved in ACC coactivity
262 formation. ACC coactivity code could rely on synaptic inputs from the connected upstream
263 medial entorhinal cortex (MEC) which is thought to be involved in transitive inference[43,44]. We
264 tested the sufficiency of such co-activation to elicit inferential behaviour from inadequate
265 training. Mice were injected into MEC with AAV9 encoding light-sensitive neuronal activator
266 (oChIEF) under the control of human synapsin (hSyn) 1 promoter (Fig. 5a). Mice were exposed
267 to an incomplete/modified protocol of the transitive inference task, in which the randomized

268 training, which is necessary to create inference (Fig. 1d, e), was replaced with optogenetic
269 activation of axonal terminals of the MEC neurons in the ACC at 4 Hz during either NREM or
270 REM sleep (Fig. 5b, c, and Extended Data Fig. 6b). All groups achieved the criterion for correct
271 performance during training of the premises (Fig. 5d). Without both randomized training and
272 MEC→ACC circuit activation, mice did not infer correctly, as demonstrated by a number of
273 correct trials that was not significantly different from chance level in the B and D context tests
274 (Fig. 5e). In contrast, artificial activation of the MEC→ACC network during REM, but not
275 NREM, sleep resulted in inference in T2, T3, and T4, in which mice exhibited significantly
276 more correct trials than those seen in T1, and significantly higher than the chance level; faster
277 selection of the rewarded context was also found (Fig. 5e, f, and Extended Data Fig. 8). These
278 results highlight the dissociable contribution of sleep stages (NREM and REM sleep) in
279 inference processing, and indicates that activating the cortical network during REM sleep is
280 sufficient for the creation of novel conclusions. All groups were proficient during testing of the
281 non-inference and the premise pairs (Extended Data Fig. 2d).
282

283 **Discussion**

284 Our study clarifies the superiority of the subconscious brain over the conscious brain in
285 restructuring existing stores of information before abstracting logical inference. During sleep,
286 multiple related memories were connected to construct a knowledge structure, which facilitated
287 innovative inference, a capacity that was not present shortly after learning. The discrepancy in
288 the performance after awake and sleep manipulations indicates the necessity of offline, but not
289 online, cortical activity to trigger inference. Sleep deprivation and optogenetic inhibition
290 experiments revealed the ability to interfere with the emergence of inference while preserving
291 memories of the original premises, thereby suggesting that stored knowledge and inferential
292 information have unique representations and/or distinct locations in the brain. The artificial

293 induction of inference by initiating communication between the MEC and ACC during REM
294 sleep implies that the dynamic interplay between cortical neural codes for related experiences
295 is critically important for the emergence of inferential behaviour.

296 Our study demonstrates that offline brain activity allows the abstraction of new
297 information from previous experiences, which differs from previous findings showing the
298 online emergence of inferential knowledge during subsequent experiences[38,45]. Furthermore,
299 causal evidence for the link between inference and offline brain activity has been lacking[38,45].
300 Our study demonstrates the offline and spontaneous emergence of inference without prior
301 priming, and provides causal evidence for the necessity and sufficiency of cortical activity
302 during sleep to inspire inferential knowledge.

303 REM sleep is characterized by vivid dreams[26] and could be initiated by activating
304 specific dopaminergic neurons in amygdala[46]. Prior investigations into the role of REM sleep
305 in cognition has found that it is necessary for memory consolidation[10] and could be involved
306 in creative problem solving by enhancing the formation of associative networks[23,26]. Here, we
307 present evidence of a causal link between REM sleep and creativity using loss and gain of
308 function experiments. Activating the MEC→ACC network at 4 Hz during REM sleep may
309 provide an ideal setting for dreaming the inference, thus leading to innovative decisions. This
310 suggestion is consistent with a previous study demonstrating that 4 Hz oscillations, dominant
311 in PFC, were phase coupled with theta rhythm, leading to modulation of neuronal spikes in the
312 PFC; hence supporting the processing of information[47]. Since theta rhythm (4-8 Hz) and
313 network oscillations support transient synchronization between brain regions[47], we hypothesize
314 that artificial stimulation of MEC→ACC network at 4 Hz may mimic the physiological circuit
315 mechanism of inference emergence.

316 The dissociable roles of REM and NREM sleep in processing the inference suggest that
317 there are distinct offline mechanisms underlying the formation of knowledge networks. Since

NREM sleep precedes REM sleep, we propose that NREM sleep prepares the knowledge network for REM-induced restructuring and the creation of novel associations[26]. This may explain why NREM sleep is crucial, but not sufficient, for the emergence of inference. The greater contribution of REM sleep over NREM sleep in inference development supports earlier findings that performance in anagram word puzzles is better after awakening from REM sleep than after awakening from NREM sleep[48]. Our Ca2+ imaging data suggests that NREM sleep may connect and organize the learned information in hierarchy, while REM sleep may build and stabilize the inference representation by creating new connections with the learned knowledge through co-reactivating their representations (Extended Data Fig. 9).

Ca2+ imaging unveiled a coactivity coding logic during offline state, which may link temporally segregated events and organize them in hierarchical order, allowing for building new information for future use. This demonstration is consistent with a previous study showing that synchronized offline reactivations are necessary for assimilating two subtly related memories, and eventually revealing the implicit commonality between them[42]. These data indicate that offline coactivation coding could underlie sleep-triggered creativity.

The capacity of REM sleep to facilitate inference from inadequate knowledge could inspire the development of novel approaches to boost cognitive performance. A recent study reported that dopamine signalling in amygdala is crucial for the transition from NREM to REM sleep[46]. Taken together, our study shed light on the mechanism of intellectual and cognitive impairments that occur in diseases that involve abnormalities in dopamine signalling like Parkinson's disease and Attention-deficit hyperactivity disorder. The ability of REM sleep to flexibly restructure our knowledge could offer new behavioural repertoires to facilitate higher-order brain functions, such as implicit learning, decision making, and creative thinking.

METHOD

343 **Animals**

344 Naïve wild-type male C57BL/6J mice were purchased from Sankyo Labo Service Co. Inc.
345 (Tokyo, Japan) and maintained on a 12 h light/dark cycle at a controlled temperature (24°C ±
346 3°C) and humidity (55% ± 5%) with free access to food and water. Mice used in behavioural
347 experiments were 14–20 weeks old. All experimental procedures with animals were congruent
348 with the guidelines of the National Institutes of Health. The Animal Care and Use Committee
349 of the University of Toyama approved all animal experiments.

350

351 **Viral constructs**

352 For the optogenetic inhibition experiment (Fig. 2 and Extended Data Fig. 5), the AAV viral
353 vector AAV-CaMKII-ArchT-eYFP (3.15×10^{13} vg/mL) was used. pAAV-CaMKII-ArchT-
354 eYFP was kindly donated by Dr. K. Deisseroth. The recombinant AAV9 production was
355 performed using a minimal purification method, and viral genomic titre was subsequently
356 calculated as described previously[49]. Briefly, pAAV recombinant vector was produced using
357 HEK293 T cells (AAV293; 240073, Agilent Tech, CA, USA) cultured in 15 cm dishes
358 (Corning, NY, USA). Cultured cells were maintained in Dulbecco's Modified Eagle Medium
359 (D-MEM) (11995-065, GIBCO life technologies, USA) supplemented with 10% fetal bovine
360 serum (FBS) (10270106, GIBCO life technologies, USA), 1% 2 mM L-Glutamine (25030-149,
361 GIBCO Life Technologies, USA), 1% 10 mM non-essential amino acid (MEM NEAA 100x,
362 11140-050, GIBCO Life Technologies, USA), and 1% (100x) penicillin-streptomycin solution
363 (15140-148, GIBCO Life Technologies, USA). Confluent (70%) HEK293 T cells were
364 transfected using medium containing the constructed expression vector, pRep/Cap, and
365 pHelper (240071, Agilent Technologies, Santa Clara, CA, USA) mixed with the transfection
366 reagent polyethyleneimine hydrochloride (PEI Max, 24765-1, Polysciences, Inc., Warrington,
367 PA, USA) at a 1:2 ratio (W/V). After 24 h, the transfection medium was discarded, and cells

368 were incubated for another 5 days in an FBS-free maintenance medium. On day 6, the AAV-
369 containing medium was collected and purified from cell debris using a 0.45 μm Millex-HV
370 syringe filter (SLHV033RS, Merck Millipore, Germany). The filtered medium was
371 concentrated and diluted with D-PBS (14190-144, GIBCO Life Technologies, USA) twice
372 using the Vivaspin 20 column (VS2041, Sartorius, Germany) after blocking the column
373 membrane with 1% bovine serum albumin (01862-87, Nacalai Tesque, Inc., Japan) in PBS. To
374 further calculate the titre, degradation of any residual cDNA in the viral solution from
375 production was first assured by benzonase nuclease treatment (70746, Merck Millipore,
376 Germany). Subsequently, viral genomic DNA was obtained after digestion with proteinase K
377 (162-22751, FUJIFILM Wako Pure Chemical, Osaka, Japan), extraction with
378 phenol/chloroform/isoamyl alcohol 25:24:1 v/v, then precipitation with isopropanol and final
379 dissolution in TE buffer (10 mM Tris [pH 8.0], 1 mM EDTA). Titre quantification for each
380 viral solution, referenced to that of the corresponding expression plasmid, was done by real-
381 time quantitative PCR (qPCR) using THUDERBIRD SYBR qPCR Master Mix (QRS-201,
382 Toyobo Co., Ltd, Japan) with the primers 5′-GGAACCCCTAGTGATGGAGTT-3′ and 5′-
383 CGGCCTCAGTGAGCGA-3′ targeting the inverted terminal repeat (ITR) sequence. The
384 cycling parameters were adjusted as follows: initial denaturation at 95°C for 60 sec, followed
385 by 40 cycles of 95°C for 15 sec and 60°C for 30 sec.

386 For the *in vivo* Ca^{2+} imaging experiment (Fig. 3, 4), the AAV viral vector AAV-Syn-
387 janelia-GCaMP7b (8.36×10^{13} vg/mL) was used. The pAAV-Syn-janelia-GCaMP7b[50] was
388 purchased from Addgene (Cambridge, MA, Plasmid #104489). The recombinant AAV9
389 production was performed using a minimal purification method, and viral genomic titre was
390 subsequently calculated as described above and previously[49].

391 For the optogenetic activation experiment (Fig. 5), the AAV viral vector AAV-hSyn1-
392 oChIEF-tdTomato (2.1×10^{13} vg/mL) was used. pAAV-hSyn1-oChIEF-tdTomato was

purchased from Addgene (Cambridge, MA, Plasmid #50977). Recombinant AAV vectors were produced by transient transfection of HEK293 cells with the vector plasmid, an AAV3 rep and AAV9 vp expression plasmid, and an adenoviral helper plasmid, pHelper (Agilent Technologies, Santa Clara, CA), as previously described[51,52].

Surgery

Mice (10–14 weeks old) were given an intraperitoneal anaesthesia injection containing 0.75 mg/kg medetomidine (Domitor; Nippon Zenyaku Kogyo Co., Ltd., Japan), 4.0 mg/kg midazolam (Fuji Pharma Co., Ltd., Japan), and 5.0 mg/kg butorphanol (Vetorphale, Meiji Seika Pharma Co., Ltd., Japan) before being placed, when sedated, on a stereotactic apparatus (Narishige, Tokyo, Japan). After surgery, an intramuscular injection of 1.5 mg/kg atipamezole (Antisedan; Nippon Zenyaku Kogyo Co., Japan), an antagonist of medetomidine, was administered to boost recovery from sedation. Mice were home caged for 3 weeks to recover from surgery before initiating behavioural experiments. All virus injections were done using a 10 μL Hamilton syringe (80030, Hamilton, USA) that was fitted with a mineral oil-filled glass needle and wired to an automated motorized microinjector IMS-20 (Narishige, Japan).

For the optogenetic inhibition experiments (Fig. 2 and Extended Data Fig. 5), 500 nL of AAV viral vector were injected at 100 nL min−1 bilaterally into either the ACC (from bregma: +0.3 mm anteroposterior [AP], ±0.35 mm mediolateral [ML]; from the skull surface: +1.5 mm dorsoventral [DV]) or prelimbic cortex (PL) (from bregma: +2.0 mm AP, ±0.35 mm ML; from the skull surface: +1.8 mm DV). The glass injection tip was maintained after injection at the target coordinates for an additional 5 min before being removed. Then, a double-guide cannula (C2002GS-5-0.7/SPC, diameter 0.29 mm, Plastics One Inc., USA) composed of two 0.7 mm-spaced stainless-steel pipes protruding for 2 mm from the plastic cannula body was bilaterally inserted either 1.0 mm ventral to the skull surface at the ACC coordinates or 1.3 mm ventral to

418 the skull surface at the PL coordinates. Guide cannulas were fixed using dental cement
419 (Provinice, Shofu Inc., Japan) that was used to fix micro-screws that were anchored into the
420 skull near bregma and lambda. After complete fixation, a dummy cannula (C2002DCS-5-
421 0.7/SPC, protrusion 0 mm, Plastics One Inc., USA) was attached to the guide cannula to protect
422 from particulate matter.

423 In parallel, a custom-built electroencephalogram/electromyography (EEG/EMG) 5-pin
424 system was installed into the skull as previously described[40]. Briefly, electrodes were screwed
425 into the skull over the parietal cortex for EEG recording, over the right cerebellar cortex as a
426 ground, and over the left cerebellar cortex as a reference. Additionally, two wires were
427 implanted into the neck muscle for EMG recording. Finally, dental cement was used to fix all
428 system screws in place.

429 For the optogenetic activation experiment (Fig. 5), 500 nL of the AAV viral vector was
430 injected at 100 nL min−1 bilaterally into the MEC (from bregma: +4.8 mm AP, ±3.3 mm ML,
431 +3.3 mm DV). The remaining procedure was as described earlier in the optogenetic inhibition
432 section.

433 For the Ca^{2+} imaging experiment (Fig. 3, 4), 500 nL of AAV_9-CaMKII::G-CaMP7 was
434 injected at 100 nL min^{-1} unilaterally into the left ACC (+1.0 mm AP, +0.35 mm ML, +1.5 mm
435 DV). After 2 weeks of recovery from AAV injection surgery, re-anesthetized mice were placed
436 once again on a stereotactic apparatus to implant a gradient index (GRIN) lens[8,42,53] (0.5 mm
437 diameter, 4 mm length; Inscopix Inc., USA) into the centre of injection (from the skull surface:
438 +1.2 mm DV) using custom-made forceps attached to a manipulator (Narishige, Japan). A low-
439 temperature cautery was used to emulsify bone wax into the gaps between the GRIN lens and
440 the skull, and then the lens was anchored in place using dental cement. Additionally, a custom-
441 built EEG/EMG 5-pin system was installed and cemented into the skull, as mentioned earlier.
442 Three weeks after GRIN implantation, mice were re-anesthetized and placed back onto the

443 stereotactic apparatus to set a baseplate (Inscopix Inc.), as described previously[42,53]. In brief, a
444 Gripper (Inscopix Inc.) holding a baseplate attached to a miniature microscope (nVista HD v3;
445 Inscopix, Inc.) was lowered over the previously set GRIN lens until visualization of clear
446 vasculature was possible, indicating the optimum focal plane. Dental cement was then applied
447 to fix the baseplate in position to preserve the optimal focal plane. Mice recovered from surgery
448 in their home cages for 1 week before behavioural imaging experiments began.
449

450 **Transitive inference task**

451 The behavioural experiments were done in soundproof room. The arena consists of 5 different
452 contexts (A, B, C, D, and E; Fig. 1a). Context A was a grey triangle (200 mm length × 300 mm
453 height) with a smooth, grey acrylic floor and walls without any patterns. Context B was a grey
454 square (200 mm length × 200 mm width × 300 mm height) with a green plastic floor with a
455 pointy texture and walls without any patterns. Context C was a blue square (200 mm length ×
456 200 mm width × 300 mm height) with a smooth, blue acrylic floor and walls without patterns.
457 Context D was a transparent square (200 mm length × 200 mm width × 300 mm height) with
458 a spongy, orange floor and walls that were covered with a characteristic pattern (black circles
459 on a white background). Context E was a transparent triangle (200 mm length × 300 mm height)
460 with a smooth, transparent acrylic floor and walls that were covered with a characteristic
461 pattern (black vertical lines on a white background).

462 Food restriction: Mice were kept under a food restriction protocol during the task. Mice
463 were provided with one 3 g food pellet and one 0.05 g sucrose tablet per day until mice reach
464 80–85% of their original weight. The sucrose tablets were put in a small Petri dish inside the
465 home cage during the first two stages (food restriction and arena habituation); the dish was
466 removed after starting the training stage and was never put it back, which served to teach mice

467 that they would no longer receive any sucrose tablets in the home cage and the only way to
468 receive the reward in the contexts was to perform the task correctly.

469 Arena habituation: On the first day, mice were put in each context separately for 5 min.
470 The contexts were closed to force mice to explore each context for the entire 5 min. The
471 exposure to the contexts was random across mice (for example, one mouse was placed in A
472 then C then D then B then E, and another mouse was placed in C then B then E then A then D).
473 On the second and third days, all contexts were open and mice were put in the start point for
474 free exploration of the whole arena for 15 min.

475 Training: The 14-day training phase was divided into 4 consecutive days for the first two
476 pairs, 4 days for the other two pairs, 2 days reinforcement, and 4 days randomization. Every
477 day, mice were exposed to two sessions, and each session consisted of five trials for a premise
478 pair without inter-trial intervals. The four premise pairs were A > B, B > C, C > D, and D > E.
479 Therefore, the hierarchy was A > B > C > D > E. For the incomplete hierarchy experiment
480 (Extended Data Fig. 4), the four premise pairs were A > B, B > C, E > D, and D > C. Therefore,
481 the hierarchies were A > B > C and E > D > C. Premise pair training was considered successful
482 when mice reached 80% correctness.

483 In the first trial of every session, mice were put at the starting point and allowed to explore
484 the arena and enter the two contexts to identify the learned pair. After entering both contexts
485 once, if they entered the correct context again and remained there for more than 10 sec, they
486 received the sucrose tablet, and the trial ended after the tablet had been consumed. If they
487 stayed in the non-rewarded context (wrong choice) for more than 10 sec, the trial ended, and
488 in the next correct trial they received the sucrose tablet after 20 sec (rather than 10 sec). After
489 each trial, mice were directly returned to the starting point to start the next trial without any
490 inter-trial interval. After completing all trials, mice were returned to their home cage for 30

min before starting the next session. After finishing two sessions, mice returned to their home cages and received a 2-g food pellet.

For randomization during training, mice were exposed to new combinations of premise pairs everyday for 4 days. These combinations were different from those presented during the initial training and reinforcement. For example, (A & B) pair was co-presented with (B & C) pair on the same day during the initial training and reinforcement, while during randomization stage (A & B) pair was co-presented with (C & D) and (D & E) pairs on two different days; and the same was applied on the other pairs to ensure the complete interaction between all premise pairs. The order of presenting the premise pairs is different across animals within the same group (Table 1). This is different from training with reinforcement, in which the (A & B) pair is usually presented with the (B & C) pair, and the (C & D) pair is usually presented with the (D & E) pair on the same day.

For the optogenetic activation experiment (Fig. 5 and Extended Data Fig. 8), training was done for 10 days only without the 4 days of randomization.

Table 1: Example of the order of presenting the premise pairs during randomization stage

Randomization Day #	**1**	**2**	**3**	**4**
Day # in the protocol	**Day # 11**	**Day # 12**	**Day # 13**	**Day # 14**
Mouse # 1	A > B C > D	B > C C > D	A > B D > E	B > C D > E
Mouse # 2	A > B D > E	A > B C > D	B > C D > E	B > C C > D
Mouse # 3	B > C C > D	B > C D > E	A > B D > E	A > B C > D

Testing: After the training phase, mice were exposed to two types of testing for 4 consecutive days. The inference test utilized a novel pair (B & D), while the non-inference test utilized another novel pair (A & E). Test 1 was done on the last day of training, while tests 2, 3, and 4 were done on the following 3 days.

511 Every day, mice were exposed to two sessions, each of which consisted of two trials for
512 each test without any inter-trial intervals. After completing all trials, mice were returned to the
513 home cage for 30 min before starting the next session. The protocol of test sessions was the
514 same as for the training sessions. When they made the correct choice, mice were rewarded with
515 a sucrose tablet in context B, except for the inference group (Fig. 1f) and both awake and sleep
516 groups (Extended Data Fig. 5). Both the B and D contexts were square and located at the end
517 of the arena (the same distance from the starting point) to avoid any preference that was due to
518 geometry and distance from the starting point. Performance during the B and D test was also
519 not due to right or left training preferences, because the design of the premise pairs was based
520 on an equal distribution of right and left preferences (the correct choice was located to the left
521 in two pairs and to the right in the other two pairs). After completing the inference and non-
522 inference tests, mice were tested with the original premise pairs to confirm that the performance
523 during the inference test was due to remembering the original memories. The arena was cleaned
524 using water and 70% ethanol after each subject. Sleep deprivation (Fig. 1) was done for 4 h by
525 gentle touching of the home cage after test sessions (after T1, T2, T3, and T4).
526 For the optogenetic inhibition experiments (Fig. 2 and Extended Data Fig. 5), optogenetic
527 inhibition of the ACC or PL was induced during wakefulness or sleep in a 4 h session. On each
528 testing day, immediately after the test sessions, mice were anesthetized using isoflurane and
529 two branch-type optical fibres (internal diameter, 0.25 mm) were inserted and fitted into their
530 housing with a cap, which anchored the inserted optical fibres with screws around the guide
531 cannula. The tip of the optical fibre protruded 0.2 mm below the guide cannula (ACC, DV 1.2
532 mm from the skull surface; PL, DV 1.5 mm from the skull surface). Mice attached to the optic
533 fibres were then placed in a sleep box and simultaneously connected to an EEG/EMG recording
534 unit and an optical swivel wired to a laser unit (9–12 mW, 589 nm). The delivery of continuous
535 light was manually controlled. After the session, mice were detached from the EEG/EMG

536 recording and light delivery systems and the fibres were removed from the cannula under
537 anaesthesia.

538 For the *in vivo* Ca^{2+} imaging experiment (Fig. 3, 4), attachment and removal of the
539 microendoscope was performed under 3% isoflurane anesthesia. Mice attached to the
540 microendoscope were returned to their home cages to recover for at least 30 min before and
541 after the behavioral session. Three days before context habituation sessions, mice were
542 habituated to the microendoscope attachment for 10 min per day in their home cages. Calcium
543 imaging data acquisition started from the last day of context habituation. Mice were exposed
544 to the above-mentioned behavioural protocol with slight modification in the initial training
545 stage. Mice were exposed to two particular premise pairs for 2 successive days, then they
546 encountered a single premise pair per day on the subsequent 2 days to collect the corresponding
547 Ca2+ data of each premise pair on a separate day. Offline Ca2+ imaging data was collected
548 from the sleep period (NREM 1 & REM 1) after contexts habituation, the awake session after
549 Test 1 (Day 24) and the sleep period (NREM 2 & REM 2) after Test 1. Ca2+ imaging data was
550 collected from the first 2 min of NREM sleep (single NREM epoch that lasts for more than 2
551 min) and from the first 2 min of REM sleep (multiple REM epochs; number of epochs across
552 animals is 3±1).

553 For the optogenetic activation experiment (Fig. 5), optogenetic activation to MEC
554 terminals in the ACC was performed during NREM or REM sleep for two consecutive days.
555 One day after test 1, mice were anesthetized using isoflurane and two branch-type optical fibres
556 (internal diameter, 0.25 mm) were inserted and fitted into their housing with a cap, which
557 anchored the inserted optical fibres by screws around the guide cannula. The tip of the optical
558 fibre protruded 0.2 mm below the guide cannula (DV 1.2 mm from the skull surface). Mice
559 attached to the optic fibres were then placed in a sleep box, and simultaneously connected to
560 an EEG/EMG recording unit and an optical swivel wired to a laser unit (9–12 mW, 473 nm).

561 The delivery of laser stimulation (4 Hz, 15 msec pulse width) was manually controlled using a
562 schedule stimulator in time-lapse mode (Master-8 pulse stimulator, A.M.P.I.). In REM-
563 stimulated mice, 4 Hz light stimulation was delivered during all REM sleep that occurred
564 within the 4 h sleep session; the total duration of light stimulation was less than 7 min per
565 mouse. For NREM-stimulated mice, light stimulation was delivered for a maximum of 3 min
566 per epoch with a 3 min inter-epoch interval. After the session, the mice were detached from the
567 EEG/EMG recording and light delivery systems and the fibres were removed from the cannula
568 under anaesthesia.

569 For the optogenetic activation experiment (Extended Data Fig. 8), the procedure was the
570 same as that described in the previous paragraph, related to Fig. 5, with a modification in the
571 stimulation protocol; the total duration of light stimulation was modified to be less than 7 min
572 per mouse, with a maximum of 3 min per epoch. This modification was done to avoid
573 prolonged light stimulation and to mimic the protocol used in REM-stimulated animals.

574

575 **Behavioural analysis**

576 All sessions were captured with an overhead web camera (Logitech HD pro C920) mounted on
577 a vertical stand. The time spent in each context during the habituation phase was counted.
578 During training and testing, the trial was considered to be correct if mice spent > 10 sec in the
579 assigned context. The percent of correct trials during training and testing sessions was
580 calculated as follows: % correct trials = (number of correct trials / total number of trials) * 100.
581 We set 80% correct trials during the training phase as the criterion for successful learning of
582 the premise pairs.

583

584 ***In vivo* Ca^{2+} imaging data acquisition and analyses**

585 Ca^{2+} signals produced from G-CaMP7 protein were captured at 20 Hz with nVista acquisition
586 software (Inscopix, CA, USA) at the maximum gain and optimal power of LED of nVistaHD.
587 Ca^{2+} imaging movie recordings of all behavioural sessions were then extracted from nVista
588 Data acquisition (DAQ) box (Inscopix, CA, USA). Using Inscopix data processing software
589 (Inscopix), movies were temporally stitched together to create a full movie that contained
590 recordings of all sessions across days, which were spatially down-sampled (2x), and then
591 corrected for across-session motion artefacts against a reference frame that was chosen from
592 any session that had a clear landmark "vasculature". Further motion correction was then
593 applied using Inscopix Mosaic software, as previously described[8]. The full movie was then
594 temporally divided into the individual sessions using Inscopix Mosaic software. Each movie
595 of individual sessions was then low bandpass filtered using Fiji software (NIH) to reduce noise,
596 as described previously[8]. The fluorescence signal intensity change ($\Delta F/F$) for each session was
597 subsequently calculated using Inscopix Mosaic software according to the formula $\Delta F/F = (F -$
598 $Fm)/Fm$, where F represents each frame's fluorescence and Fm is the mean fluorescence for
599 the whole session's movie. Afterwards, movies representing each session were re-concatenated
600 again to generate the full movie for all sessions in the $\Delta F/F$ format. Finally, cells were identified
601 using an automatic sorting system, HOTARU, and each cell's Ca^{2+} signals over time were
602 extracted in a (Ď; time × neuron) matrix format, as previously described[8]. Further processing
603 was performed using codes written in MATLAB to remove the low frequency fluctuation and
604 background noise by subjecting output Ca^{2+} signals to high-pass filtering with a 0.01 Hz
605 threshold, and to then calculate z-scores from the mean of each session, whereby negative
606 values were replaced with zero. Ca^{2+} events were finally extracted after cutting off signals
607 below 3 SD from the local maxima of the $\Delta F/F$ signal of each session.
608
609 **Neural ensembles analyses**

610 Neural ensembles representing a range of neurons co-firing together was calculated using
611 unsupervised statistical method using PCA-ICA analysis as previously described[54,55]. Initially,
612 frames were binned to 0.2 s, then to prevent the bias due to differences in the average firing
613 rates, neuronal Ca^{2+} transients were normalized for each neuron by a z-score transform:

614 $$z_{i,b} = \frac{x_{i,b} - \mu_{x_i}}{\sigma_{x_i}}$$

615 where for neuron i, $z_{i,b}$ is its z-scored Ca^{2+} transients in bin b, $x_{i,b}$ its Ca^{2+} transients in bin b,
616 μ_{x_i} its mean Ca^{2+} transients across all bins and σ_{x_i} the s.d. of its Ca^{2+} transients. The calculation
617 of the principal components and the determination of the number of significant components
618 were carried out according to previously presented methods.

619 To quantify the extent to which ACC neurons contribute to the formation of neuronal
620 ensembles, we applied reconstruction ICA to significant principal components as described
621 previously[54,55]. Ensemble activation strength was then calculated through:

622 $$R_k(t) = z(t)^T P_k z(t)$$

623 where $R_k(t)$, the activation strength of ensemble k at time t
624 Wilcoxon rank-sum test was then used to reveal which of the identified ensembles are
625 significantly different between reference and target sessions. $R_k(t) > 2$ were set as a threshold
626 for ensembles to be included in the test.

627

628 **Coactivity index analysis**

629 The coactivity index was calculated as described previously[53]. The z-scores of neuronal Ca2+
630 events were calculated as described above. The z-scores were binarized by thresholding (> 3
631 Standard Deviations from the ΔF/F signal) at the local maxima of the ΔF/F signal, and then
632 were temporally down-sampled from 20 to 5 Hz data (200 ms binning). Subsequently, the
633 coactivation index consisting of the number of synchronized activities among neurons -

634 constituting different patterns from different sessions- in each 200 ms time window, was
635 calculated and normalized in each behavioural session. The following equations are used for
636 the calculations of pairwise, quadruple and quintuple coactivity index:

637
638
$$Pairwise\ Coactivity = \frac{1}{\mathrm{T}} \frac{\sum_{t=1}^{T} n_{SessionA}(t).\, n_{SessionB}(t)}{N_{SessionA}.\, N_{SessionB}}$$

639
640
641
$$Quadruple\ Coactivity = \frac{1}{\mathrm{T}} \frac{\sum_{t=1}^{T} n_{SessionA}(t).\, n_{SessionB}(t)\,.\, n_{SessionC}(t).\, n_{SessionD}(t)}{N_{SessionA}.\, N_{SessionB}.\, N_{SessionC}.\, N_{SessionD}}$$

642
643
644
$$Qunituple\ Coativity = \frac{1}{\mathrm{T}} \frac{\sum_{t=1}^{T} n_{SessionA}(t).\, n_{SessionB}(t)\,.\, n_{SessionC}(t).\, n_{SessionD}(t).\, n_{SessionE}(t)}{N_{SessionA}.\, N_{SessionB}.\, N_{SessionC}.\, N_{SessionD}.\, N_{SessionE}}$$

645

646 Where A, B, C, D & E are different behavioral sessions; $n_{SessionA}(t)$ is the number of cells,
647 constituting significant patterns in Session A, that were active in the time bin t; $N_{SessionA}$ is the
648 total number of Session A cells; and T is the total number of time bins for each session.
649 To exclude the possibility that the observed coactivity results from the difference in activities
650 among cells and sessions, we generated shuffled data (1,000 surrogate values) by using the
651 "circshift function of MATLAB"[56].

652

653 **Sleep detection data acquisition and online state detection**

654 All EEG/EMG recordings were performed using OpenEx Software Suite (Tucker Davis
655 Technologies, USA), as previously described[40] with minor modifications. Briefly, EEG signals
656 were amplified and filtered at 1–40 Hz, while 65–150 Hz was used for EMG; signals were then
657 digitized at a sampling rate of 508.6 Hz. Sleep stages were differentiated using an algorithm
658 file that enabled the calculation and analysis of the EMG root mean square value (RMS), EEG
659 delta power (1–4 Hz) RMS, and EEG theta power (6–9 Hz) RMS. The EMG RMS threshold
660 was optimized according to each subject. Mice was judged to be awake when the EMG RMS

661 exceeded the set threshold value and remained unchanged for three successive 3 sec
662 checkpoints. However, when EMG RMS was lower than the threshold, sleep stage
663 differentiation was concluded based on the delta/theta (d/t) ratio value. Briefly, if the d/t ratio
664 exceeded 1 for the consecutive 9 sec checking period, the stage was classified as NREM sleep;
665 conversely, it was classified as REM sleep when it was less than 1 for a consecutive 9 sec. The
666 state classified by the program was also confirmed by the experimenter through visual
667 inspection of mouse activity and EEG delta-dominant (0.5–4 Hz) or theta-dominant (4–9 Hz)
668 waveforms. EEG/EMG traces recorded during sleep sessions were then extracted using
669 MATLAB codes.
670
671 **Histology**
672 After the optogenetic manipulation experiments, mice were deeply anesthetized with 1 mL of
673 combination anaesthesia and perfused transcardially with PBS (pH 7.4) followed by 4%
674 paraformaldehyde in PBS. The brains were extracted, then further immersed in
675 paraformaldehyde in PBS for 12–18 h at 4°C. Subsequently, fixed brains were mixed with 25%
676 sucrose in PBS for 36–48 h at 4°C before final storage at –80°C. To obtain coronal sections,
677 brains were sliced into 50 μm sections using a cryostat (Leica CM3050, Leica Biosystems) and
678 were then washed in PBS-containing 12-well culture plates (Corning, NY, USA). The sections
679 were further incubated at room temperature for 1 h with a blocking buffer (3% normal donkey
680 serum; S30, Chemicon by EMD Millipore, Billerica, MA, USA) in PBS solution containing
681 0.2% Triton X-100 and 0.05% Tween 20 (PBST). After incubation, the buffer was discarded
682 and rat anti-GFP (04404-84, GF090R, Nacalai Tesque Inc., Japan) primary antibody (1:500)
683 in blocking solution was added for further incubation at 4°C for 24–36 h. At the end of the
684 incubation period, the primary antibody was removed and sections were washed with 0.2%
685 PBST three times for 10 min each. After washing, sections were treated with a complementary

686 secondary antibody, (1:1000) donkey anti-rat IgG Alexa Fluor 488 (A21208, Molecular
687 Probes) in blocking buffer solution at room temperature for 2–3 h. Finally, the sections were
688 treated with DAPI (1 μg/mL, Roche Diagnostics, 10236276001) for nuclear staining and
689 washed with 0.2% PBST three times for 10 min each before being mounted onto glass slides
690 with ProLong Gold antifade reagent (Invitrogen).
691

692 **Confocal microscopy**

693 Images were acquired using a confocal microscope (Zeiss LSM 780, Carl Zeiss, Jena,
694 Germany) with 20× Plan-Apochromat objective lens. All parameters, such as the
695 photomultiplier tube assignments, pinhole sizes, and contrast values, were standardized within
696 each magnification and experimental condition.
697

698 **Statistics**

699 Statistical analyses were performed using Prism 8 (GraphPad Software, San Diego, CA, USA).
700 Multiple-group comparisons were performed using an ANOVA with post hoc tests, as shown
701 in the corresponding Fig. legends. Quantitative data are presented as the mean ± SEM.
702

703 **Data and Code Availability**

704 All data, codes, and resources that supported the findings of this study are available upon
705 reasonable request.
706

707 **Acknowledgments**

708 We thank Khaled Ghandour and Ali Choucry (University of Toyama) for their valuable
709 discussions and suggestions. We thank all members of the Inokuchi Laboratory for their
710 discussions and support. We thank Mika Ito and Naomi Takino (Jichi Medical University) for

their help with the production of the AAV vectors. Also, we thank Noriaki Ohkawa (Dokyyo University) for his help in providing the materials used to build the behavioural arena. We would like to thank Karl Deisseroth (Stanford University) for providing us with pAAV-CaMKII-ArchT 3.0-EYFP. We also thank Ayumu Konno and Hirokazu Hirai (Gunma University) for providing us with the virus preparation protocol.

This work was supported by the JSPS KAKENHI (grant number JP18H05213, JP23H05476), the Core Research for Evolutional Science and Technology (CREST) program (JPMJCR13W1) of the Japan Science and Technology Agency (JST), a Grant-in-Aid for Scientific Research on Innovative Areas "Memory dynamism" (JP25115002) from MEXT, and the Takeda Science Foundation to K.I.; JSPS KAKENHI (grant number JP19K16892) to K.A.; and the Uehara Memorial Foundation scholarship to M.A.; JST SPRING scholarship (grant number JPMJSP2145) to A.I.

Author contributions

K.A. and K.I. designed the experiments and wrote the manuscript. K.A., K.C., M.A. and A.I. performed the experiments. K.A. analysed the data. S.M. and R.O-S. prepared adeno-associated viruses. K.I. supervised the entire project.

Competing interests

S.M. owns equity in a company, Gene Therapy Research Institution, that commercializes the use of AAV vectors for gene therapy applications. To the extent that the work in this manuscript increases the value of these commercial holdings, S.M. has a conflict of interest. The other authors declare no competing interests.

References

1 Buzsaki, G. & Fernandez-Ruiz, A. Utility of the Idling Brain: Abstraction of New Knowledge. *Cell* **178**, 513-515 (2019). https://doi.org:10.1016/j.cell.2019.07.004

2 Ghandour, K. & Inokuchi, K. Memory reactivations during sleep. *Neurosci Res* **189**, 60-65 (2023). https://doi.org:10.1016/j.neures.2022.12.018

3 Ellenbogen, J. M., Hu, P. T., Payne, J. D., Titone, D. & Walker, M. P. Human relational memory requires time and sleep. *Proc Natl Acad Sci U S A* **104**, 7723-7728 (2007). https://doi.org:10.1073/pnas.0700094104

4 Wagner, U., Gais, S., Haider, H., Verleger, R. & Born, J. Sleep inspires insight. *Nature* **427**, 352-355 (2004). https://doi.org:10.1038/nature02223

5 Behrens, T. E. J. *et al.* What Is a Cognitive Map? Organizing Knowledge for Flexible Behavior. *Neuron* **100**, 490-509 (2018). https://doi.org:10.1016/j.neuron.2018.10.002

6 Brunamonti, E. *et al.* Neuronal Modulation in the Prefrontal Cortex in a Transitive Inference Task: Evidence of Neuronal Correlates of Mental Schema Management. *The Journal of neuroscience : the official journal of the Society for Neuroscience* **36**, 1223-1236 (2016). https://doi.org:10.1523/JNEUROSCI.1473-15.2016

7 Spalding, K. N. *et al.* Ventromedial Prefrontal Cortex Is Necessary for Normal Associative Inference and Memory Integration. *The Journal of neuroscience : the official journal of the Society for Neuroscience* **38**, 3767-3775 (2018). https://doi.org:10.1523/JNEUROSCI.2501-17.2018

8 Ghandour, K. *et al.* Orchestrated ensemble activities constitute a hippocampal memory engram. *Nat Commun* **10**, 2637 (2019). https://doi.org:10.1038/s41467-019-10683-2

9 Wilson, M. A. & McNaughton, B. L. Reactivation of hippocampal ensemble memories during sleep. *Science* **265**, 676-679 (1994). https://doi.org:10.1126/science.8036517

10 Boyce, R., Glasgow, S. D., Williams, S. & Adamantidis, A. Causal evidence for the role of REM sleep theta rhythm in contextual memory consolidation. *Science (New York, N.Y.)* **352**, 812-816 (2016). https://doi.org:10.1126/science.aad5252

11 Girardeau, G., Benchenane, K., Wiener, S. I., Buzsaki, G. & Zugaro, M. B. Selective suppression of hippocampal ripples impairs spatial memory. *Nat Neurosci* **12**, 1222-1223 (2009). https://doi.org:10.1038/nn.2384

12 Gridchyn, I., Schoenenberger, P., O'Neill, J. & Csicsvari, J. Assembly-Specific Disruption of Hippocampal Replay Leads to Selective Memory Deficit. *Neuron* **106**, 291-300 e296 (2020). https://doi.org:10.1016/j.neuron.2020.01.021

13 Diekelmann, S. & Born, J. The memory function of sleep. *Nat Rev Neurosci* **11**, 114-126 (2010). https://doi.org:10.1038/nrn2762

14 Gupta, A. S., van der Meer, M. A., Touretzky, D. S. & Redish, A. D. Hippocampal replay is not a simple function of experience. *Neuron* **65**, 695-705 (2010). https://doi.org:10.1016/j.neuron.2010.01.034

15 Olafsdottir, H. F., Barry, C., Saleem, A. B., Hassabis, D. & Spiers, H. J. Hippocampal place cells construct reward related sequences through unexplored space. *eLife* **4**, e06063 (2015). https://doi.org:10.7554/eLife.06063

16 Olafsdottir, H. F., Bush, D. & Barry, C. The Role of Hippocampal Replay in Memory and Planning. *Current biology : CB* **28**, R37-R50 (2018). https://doi.org:10.1016/j.cub.2017.10.073

17 Cousins, J. N., El-Deredy, W., Parkes, L. M., Hennies, N. & Lewis, P. A. Cued memory reactivation during slow-wave sleep promotes explicit knowledge of a motor sequence. *The Journal of neuroscience : the official journal of the Society for Neuroscience* **34**, 15870-15876 (2014). https://doi.org:10.1523/JNEUROSCI.1011-14.2014

18 Gais, S. & Born, J. Low acetylcholine during slow-wave sleep is critical for declarative memory consolidation. *Proc Natl Acad Sci U S A* **101**, 2140-2144 (2004). https://doi.org:10.1073/pnas.0305404101

19 Plihal, W. & Born, J. Effects of early and late nocturnal sleep on declarative and procedural memory. *J Cogn Neurosci* **9**, 534-547 (1997). https://doi.org:10.1162/jocn.1997.9.4.534

20 Plihal, W. & Born, J. Memory consolidation in human sleep depends on inhibition of glucocorticoid release. *Neuroreport* **10**, 2741-2747 (1999). https://doi.org:10.1097/00001756-199909090-00009

21 Walker, M. P. The role of sleep in cognition and emotion. *Annals of the New York Academy of Sciences* **1156**, 168-197 (2009). https://doi.org:10.1111/j.1749-6632.2009.04416.x

22 Wamsley, E. J., Tucker, M., Payne, J. D., Benavides, J. A. & Stickgold, R. Dreaming of a learning task is associated with enhanced sleep-dependent memory consolidation. *Current biology : CB* **20**, 850-855 (2010). https://doi.org:10.1016/j.cub.2010.03.027

23 Cai, D. J., Mednick, S. A., Harrison, E. M., Kanady, J. C. & Mednick, S. C. REM, not incubation, improves creativity by priming associative networks. *Proceedings of the National Academy of Sciences of the United States of America* **106**, 10130-10134 (2009). https://doi.org:10.1073/pnas.0900271106

24 Poe, G. R., Walsh, C. M. & Bjorness, T. E. Cognitive neuroscience of sleep. *Prog Brain Res* **185**, 1-19 (2010). https://doi.org:10.1016/B978-0-444-53702-7.00001-4

25 Brodt, S., Inostroza, M., Niethard, N. & Born, J. Sleep-A brain-state serving systems memory consolidation. *Neuron* **111**, 1050-1075 (2023). https://doi.org:10.1016/j.neuron.2023.03.005

26 Lewis, P. A., Knoblich, G. & Poe, G. How Memory Replay in Sleep Boosts Creative Problem-Solving. *Trends in cognitive sciences* **22**, 491-503 (2018). https://doi.org:10.1016/j.tics.2018.03.009

27 Bramham, C. R. & Srebro, B. Synaptic plasticity in the hippocampus is modulated by behavioral state. *Brain Res* **493**, 74-86 (1989). https://doi.org:10.1016/0006-8993(89)91001-9

28 Basheer, R. *et al.* Effects of sleep on wake-induced c-fos expression. *J Neurosci* **17**, 9746-9750 (1997).

29 Cirelli, C. & Tononi, G. Gene expression in the brain across the sleep-waking cycle. *Brain Res* **885**, 303-321 (2000). https://doi.org:10.1016/s0006-8993(00)03008-0

30 Cirelli, C. & Tononi, G. Differential expression of plasticity-related genes in waking and sleep and their regulation by the noradrenergic system. *J Neurosci* **20**, 9187-9194 (2000).

31 Pompeiano, M., Cirelli, C., Arrighi, P. & Tononi, G. c-Fos expression during wakefulness and sleep. *Neurophysiol Clin* **25**, 329-341 (1995). https://doi.org:10.1016/0987-7053(96)84906-9

32 Pompeiano, M., Cirelli, C., Ronca-Testoni, S. & Tononi, G. NGFI-A expression in the rat brain after sleep deprivation. *Brain Res Mol Brain Res* **46**, 143-153 (1997). https://doi.org:10.1016/s0169-328x(96)00295-1

33 Pompeiano, M., Cirelli, C. & Tononi, G. Immediate-early genes in spontaneous wakefulness and sleep: expression of c-fos and NGFI-A mRNA and protein. *J Sleep Res* **3**, 80-96 (1994). https://doi.org:10.1111/j.1365-2869.1994.tb00111.x

34 Ackermann, S. & Rasch, B. Differential effects of non-REM and REM sleep on memory consolidation? *Curr Neurol Neurosci Rep* **14**, 430 (2014). https://doi.org:10.1007/s11910-013-0430-8

35 Tamaki, M. *et al.* Complementary contributions of non-REM and REM sleep to visual learning. *Nat Neurosci* **23**, 1150-1156 (2020). https://doi.org:10.1038/s41593-020-0666-y

36 Pereira, S. I. R. & Lewis, P. A. The differing roles of NREM and REM sleep in the slow enhancement of skills and schemas. *Current Opinion in Physiology* **15**, 82-88 (2020). https://doi.org:https://doi.org/10.1016/j.cophys.2019.12.005

37 Preston, A. R. & Eichenbaum, H. Interplay of hippocampus and prefrontal cortex in memory. *Current biology : CB* **23**, R764-773 (2013). https://doi.org:10.1016/j.cub.2013.05.041

38 Barron, H. C. *et al.* Neuronal Computation Underlying Inferential Reasoning in Humans and Mice. *Cell* **183**, 228-243 e221 (2020). https://doi.org:10.1016/j.cell.2020.08.035

39 Zeithamova, D., Dominick, A. L. & Preston, A. R. Hippocampal and ventral medial prefrontal activation during retrieval-mediated learning supports novel inference. *Neuron* **75**, 168-179 (2012). https://doi.org:10.1016/j.neuron.2012.05.010

40 Miyamoto, D. *et al.* Top-down cortical input during NREM sleep consolidates perceptual memory. *Science* **352**, 1315-1318 (2016). https://doi.org:10.1126/science.aaf0902

41 Takekawa, T. *et al.* Automatic sorting system for large calcium imaging data. *bioRxiv*, 215145 (2017). https://doi.org:10.1101/215145

42 Aly, M. H., Abdou, K., Okubo-Suzuki, R., Nomoto, M. & Inokuchi, K. Selective engram coreactivation in idling brain inspires implicit learning. *Proc Natl Acad Sci U S A* **119**, e2201578119 (2022). https://doi.org:10.1073/pnas.2201578119

43 Dusek, J. A. & Eichenbaum, H. The hippocampus and memory for orderly stimulus relations. *Proc Natl Acad Sci U S A* **94**, 7109-7114 (1997). https://doi.org:10.1073/pnas.94.13.7109

44 Buckmaster, C. A., Eichenbaum, H., Amaral, D. G., Suzuki, W. A. & Rapp, P. R. Entorhinal cortex lesions disrupt the relational organization of memory in monkeys. *J Neurosci* **24**, 9811-9825 (2004). https://doi.org:10.1523/JNEUROSCI.1532-04.2004

45 Liu, Y., Dolan, R. J., Kurth-Nelson, Z. & Behrens, T. E. J. Human Replay Spontaneously Reorganizes Experience. *Cell* **178**, 640-652 e614 (2019). https://doi.org:10.1016/j.cell.2019.06.012

46 Hasegawa, E. *et al.* Rapid eye movement sleep is initiated by basolateral amygdala dopamine signaling in mice. *Science* **375**, 994-1000 (2022). https://doi.org:10.1126/science.abl6618

47 Fujisawa, S. & Buzsaki, G. A 4 Hz oscillation adaptively synchronizes prefrontal, VTA, and hippocampal activities. *Neuron* **72**, 153-165 (2011). https://doi.org:10.1016/j.neuron.2011.08.018

48 Walker, M. P., Liston, C., Hobson, J. A. & Stickgold, R. Cognitive flexibility across the sleep-wake cycle: REM-sleep enhancement of anagram problem solving. *Brain Res Cogn Brain Res* **14**, 317-324 (2002). https://doi.org:10.1016/s0926-6410(02)00134-9

49 Konno, A. & Hirai, H. Efficient whole brain transduction by systemic infusion of minimally purified AAV-PHP.eB. *J Neurosci Methods* **346**, 108914 (2020). https://doi.org:10.1016/j.jneumeth.2020.108914

50 Dana, H. *et al.* High-performance calcium sensors for imaging activity in neuronal populations and microcompartments. *Nat Methods* **16**, 649-657 (2019). https://doi.org:10.1038/s41592-019-0435-6

51 Iida, A., Takino, N., Miyauchi, H., Shimazaki, K. & Muramatsu, S. Systemic delivery of tyrosine-mutant AAV vectors results in robust transduction of neurons in adult mice. *Biomed Res Int* **2013**, 974819 (2013). https://doi.org:10.1155/2013/974819

52 Li, X. G. *et al.* Viral-mediated temporally controlled dopamine production in a rat model of Parkinson disease. *Mol Ther* **13**, 160-166 (2006). https://doi.org:10.1016/j.ymthe.2005.08.009

53 Nomoto, M. *et al.* Hippocampus as a sorter and reverberatory integrator of sensory inputs. *Nat Commun* **13**, 7413 (2022). https://doi.org:10.1038/s41467-022-35119-2

54 Middleton, S. J. *et al.* Altered hippocampal replay is associated with memory impairment in mice heterozygous for the Scn2a gene. *Nat Neurosci* **21**, 996-1003 (2018). https://doi.org:10.1038/s41593-018-0163-8

55 Trouche, S. *et al.* Recoding a cocaine-place memory engram to a neutral engram in the hippocampus. *Nat Neurosci* **19**, 564-567 (2016). https://doi.org:10.1038/nn.4250

56 Watrous, A. J., Miller, J., Qasim, S. E., Fried, I. & Jacobs, J. Phase-tuned neuronal firing encodes human contextual representations for navigational goals. *Elife* **7** (2018). https://doi.org:10.7554/eLife.32554

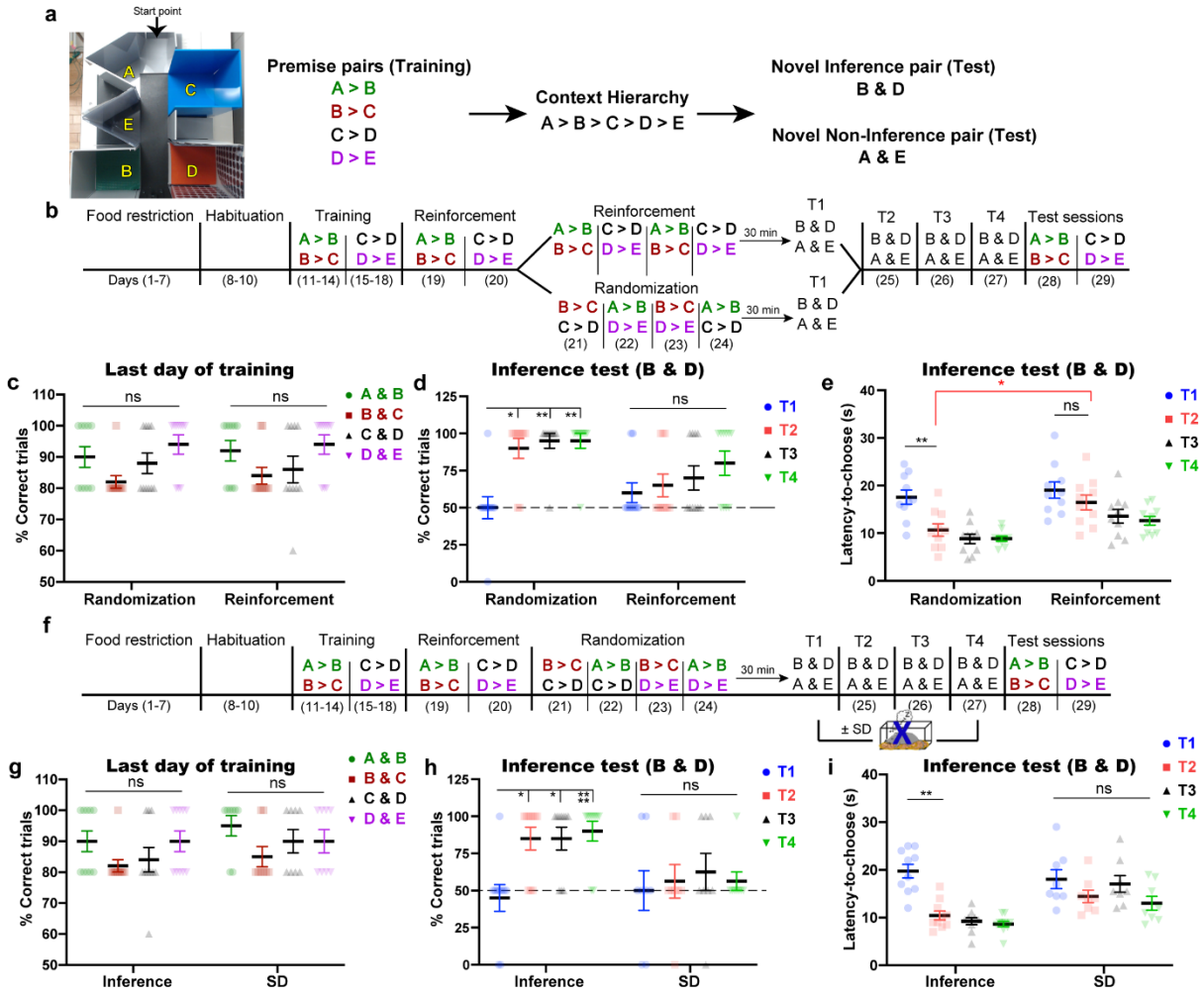

Fig. 1 | The emergence of inference requires sleep after training. a, Representative photo of the arena and the five different contexts with an arrow representing the starting point (left). The four premise pairs with the contexts' hierarchy (right). **b,** The behavioural schedule used to establish the transitive inference paradigm in mice. The contexts' hierarchy was as follows: A > B > C > D > E. The order of presentation of the premise pairs during the randomization stage is different across animals within the same group (See Methods; Table 1). **c,** Performance during the last day of training (day 14 for A > B and B > C; day 18 for C > D and D > E) for each premise pair was calculated as the percent of correct trials out of the total number of trials. **d-e,** Performance during test sessions; the percent of correct trials in the inference test (**d**), the latency time to choose in the inference test (**e**). **f,** Behavioural protocol for the transitive inference paradigm; SD, sleep deprivation. **g,** Percent of correct trials during the last day of

training (day 14 for A > B and B > C; day 18 for C > D and D > E) for each premise pair. **h-i,** Performance during test sessions; percent of correct trials during the inference test (**h**), latency time to choose during the inference test (**i**). T1, test 1; T2, test 2; T3, test 3; T4, test 4. $n = 10$ mice/group; $n = 8$ mice for the sleep deprivation (SD) group. Statistical comparisons were made using a two-way repeated-measures ANOVA with Tukey's multiple comparison test (**c-e, g-h**) and Holm-Sidak's test between groups (**e**). *$P < 0.05$; **$P < 0.01$; ****$P < 0.0001$; ns, not significant ($P > 0.05$). Data are presented as the mean ± standard error of the mean (s.e.m.).

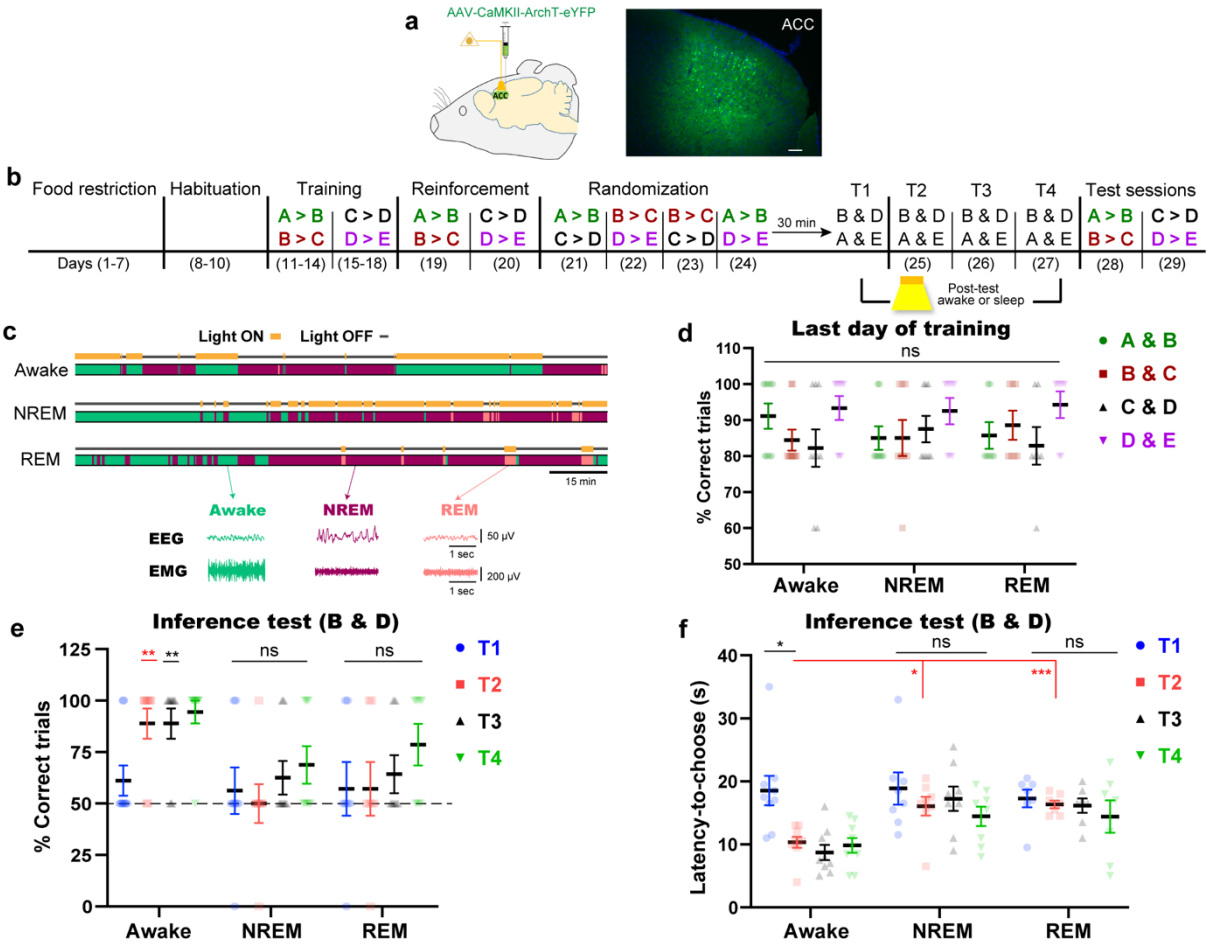

Fig. 2 | ACC computations during sleep are crucial for the emergence of inference. a, Labelling excitatory neurons of the ACC with ArchT (left), and the expression of ArchT-eYFP (green) in the ACC (right). Blue, 4′,6-diamidino-2-phenylindole (DAPI) staining. Scale bar, 100 µm. **b**, Behavioural schedule used to manipulate ACC activity during sleep and awake periods after test sessions. The order of presentation of the premise pairs during the randomization stage is different across animals within the same group (See Methods; Table 1). **c**, Diagram showing the state-specific manipulation (top) and representative electroencephalogram (EEG) and electromyography (EMG) (bottom) traces. Scale bar, 15 minutes. **d,** Performance during the last day of training (day 14 for A > B and B > C; day 18 for C > D and D > E) for each premise pair. **e-f,** Performance during test sessions; percent of correct trials during the inference test (**e**), latency time to choose during the inference test (**f**).

T1, test 1; T2, test 2; T3, test 3; T4, test 4. $n = 9$ mice for the awake group; $n = 8$ mice for the non-rapid eye movement (NREM) sleep group; $n = 7$ mice for the rapid eye movement (REM) sleep group. Statistical comparisons were made using two-way repeated-measures analysis of variance (ANOVA) with Tukey's multiple comparison test (**d-f**). In (**e**), the statistical significance denotes the comparison between performance relative to the chance level (50%). $^{*}P < 0.05$; $^{**}P < 0.01$; $^{***}P < 0.001$; ns, not significant ($P > 0.05$). Data are presented as the mean ± standard error of the mean (s.e.m.).

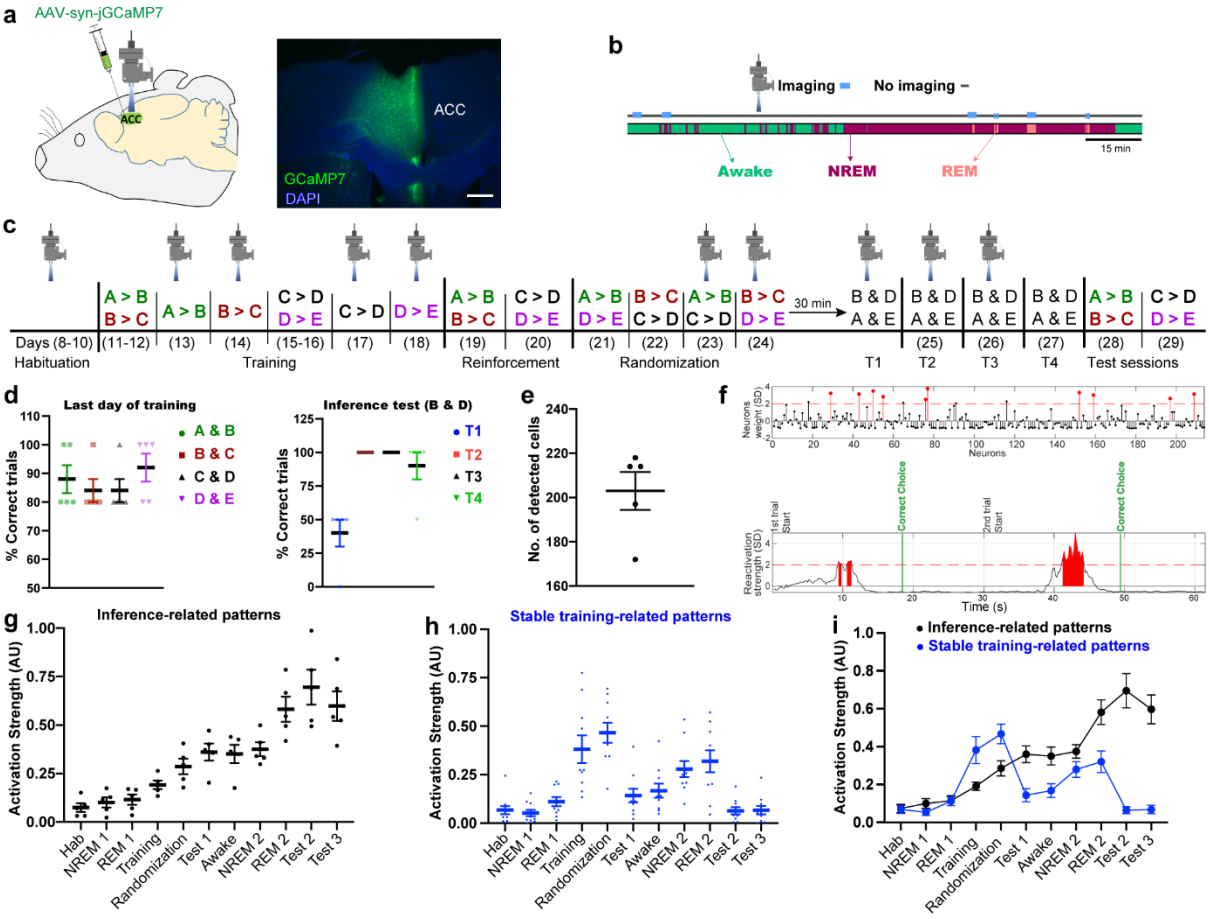

Fig. 3 | Identifying inference-related ensembles that emerge gradually and become evident during REM sleep. a, Labelling of the ACC with GCaMP7 (left), and the expression of GCaMP7 (green) in the ACC (right). Blue, 4′,6-diamidino-2-phenylindole (DAPI) staining. Scale bar, 100 µm. **b**, Diagram showing the state-specific imaging. **c,** The behavioural schedule used to capture the Ca^{2+} transients across the task. The order of presentation of the premise pairs during the randomization stage is different across animals within the same group (See Methods; Table 1). **d,** Performance during the last day of training (day 13 for A > B; day 14 for B > C; day 17 for C > D; day 18 for D > E) for each premise pair (left). Performance during test sessions (right). T1, test 1; T2, test 2; T3, test 3; T4, test 4. n = 5 mice. **e,** Total number of detected cells in each mouse. **f,** Example of ACC coactivity pattern (inference-related pattern) detected in T2 session. The pattern is represented as a vector containing the contribution

(weight) of each neuron's spiking to the coactivity defining that pattern. Neurons with a weight above 2 s.d. of the mean were referred to as members (Red) (top). The temporal appearance of the pattern with the behaviour signature (just before the correct choice) (bottom). **g-i,** Activation strength (z-scored) of inference-related patterns (**g, i**), of stable training-related patterns (**h, i**). Hab, habituation session; NREM 1, NREM sleep after last habituation session; REM 1, REM sleep after last habituation session; NREM 2, NREM sleep after T1; REM 2, REM sleep after T1. Statistical comparisons were made using two-way repeated-measures analysis of variance (ANOVA) with Dunnett's multiple comparison test (**g, h**). *$P < 0.05$; **$P < 0.01$; ns, not significant ($P > 0.05$). Data are presented as the mean ± standard error of the mean (s.e.m.).

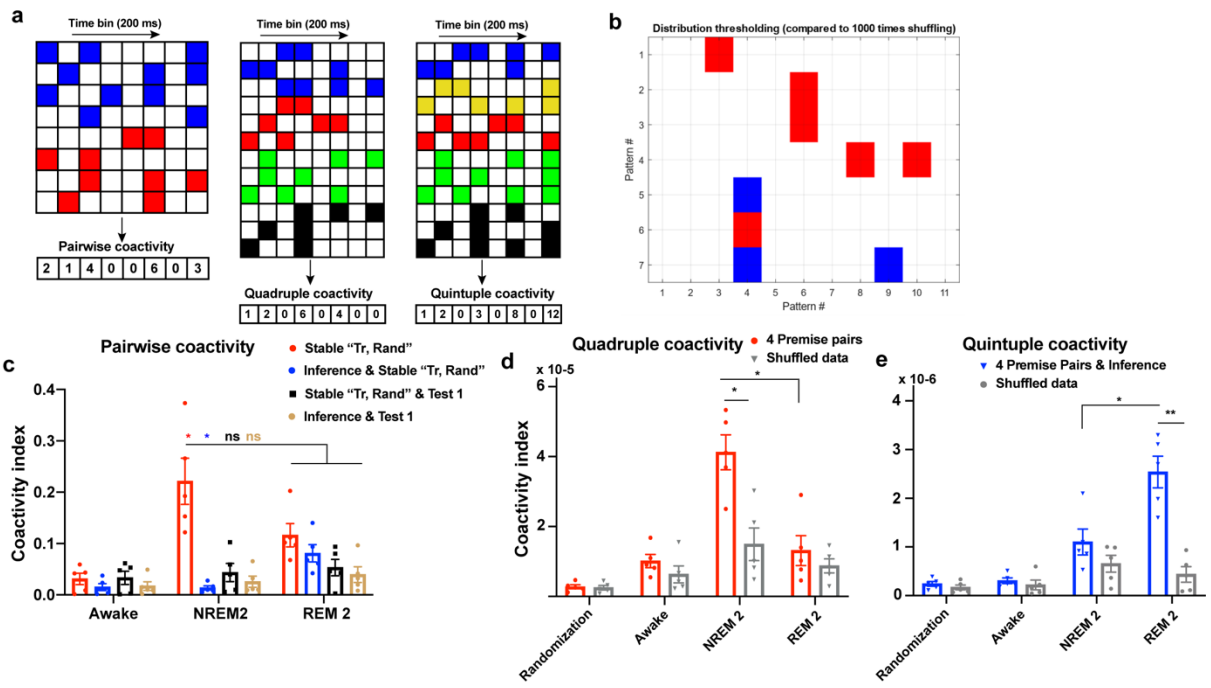

Fig. 4 | NREM and REM sleep coordinate to build synchronized inference representation with learned knowledge representation. a, Representative raster plots showing coactivity analysis. This analysis calculates coactivity by normalizing the number of synchronizations every 200 ms among different neuronal subpopulations representing different sessions. Coactivity analysis was done for neurons belonging to different patterns representing 2 sessions (Pairwise coactivity, left), representing 4 sessions (Quadruple coactivity, middle) and representing 5 sessions (Quintuple, right). **b**, Coactivity index between 2 different patterns compared to that appeared from shuffled data. Higher synchrony compared to shuffled data is represented with red color, while lower synchrony is represented with blue color. **c-e,** Coactivity index between 2 sessions (**c**), 4 sessions (**d**) and 5 sessions (**e**) with the shuffled data. Statistical comparisons were made using two-way repeated-measures analysis of variance (ANOVA) with Tukey's multiple comparison test (**c-e**). $*P < 0.05$; $**P < 0.01$; ns, not significant ($P > 0.05$). Data are presented as the mean ± standard error of the mean (s.e.m.).

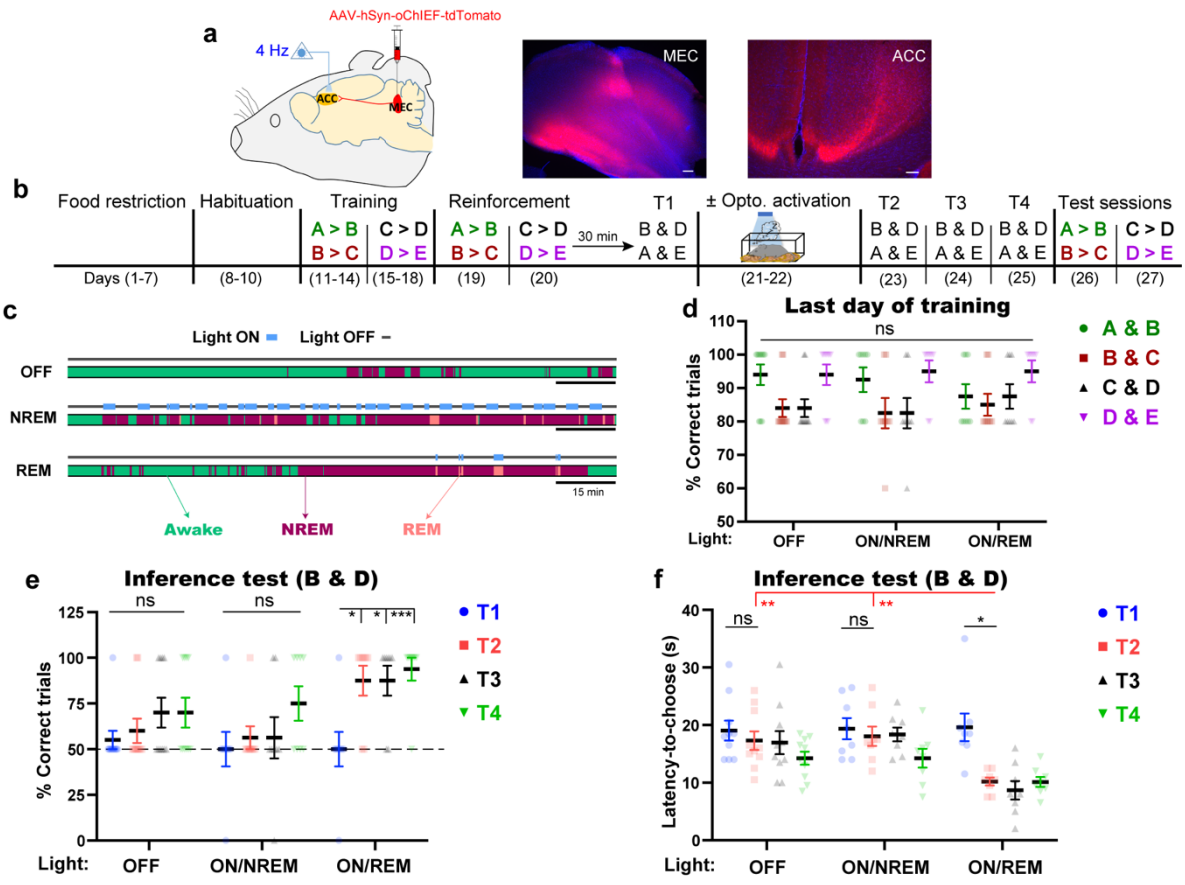

Fig. 5 | MEC→ACC crosstalk during only REM sleep is sufficient to inspire inference from inadequate training. a, The strategy for labelling MEC neurons and targeting their terminals in the ACC (left), and expression of oChIEF-tdTomato (red) in MEC neurons (middle) and their terminals in the ACC (right). Blue, 4′ ,6-diamidino-2-phenylindole (DAPI) staining. Scale bars, 100 µm. **b**, The behavioural schedule used to manipulate the MEC→ACC circuit during different sleep stages. **c**, Diagram showing the sleep stage-specific manipulation. Scale bar, 15 minutes. **d,** Performance during the last day of training (day 14 for A > B and B > C; day 18 for C > D and D > E) for each premise pair. **e-f,** Performance during test sessions; the percent of correct trials during the inference test (**e**), the latency time to choose during the inference test (**f**). T1, test 1; T2, test 2; T3, test 3; T4, test 4. n = 10 mice for the light off group; n = 8 mice for the non-rapid eye movement (NREM) sleep group; n = 8 mice for the rapid eye movement (REM) sleep group. Statistical comparisons were made using a two-way repeated-measures analysis of variance (ANOVA) (**d-f**) with Newman-Keuls multiple comparison test

978 (**e**) and Tukey's multiple comparison test (**d, f**). *$P < 0.05$; **$P < 0.01$; ****$P < 0.0001$; ns,

979 not significant ($P > 0.05$). Data are presented as the mean ± standard error of the mean (s.e.m.).

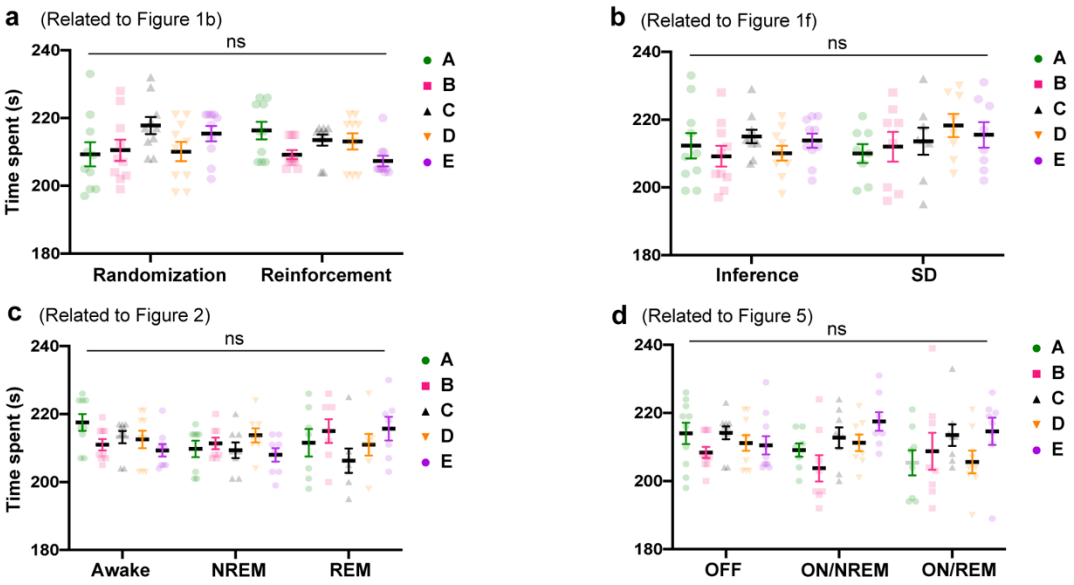

Extended Data Fig. 1 | Mice had no innate preference to any context during habituation. **a-d**, Time spent in each context during the habituation phase. The number of animals in each panel is mentioned in the corresponding Figure legend. SD, sleep deprivation; NREM, non-rapid eye movement; REM, rapid eye movement. Statistical comparisons were made using a two-way repeated-measures analysis of variance (ANOVA) with Tukey's multiple comparison test (**a-d**). ns, not significant ($P > 0.05$). Data are presented as the mean ± standard error of the mean (s.e.m.).

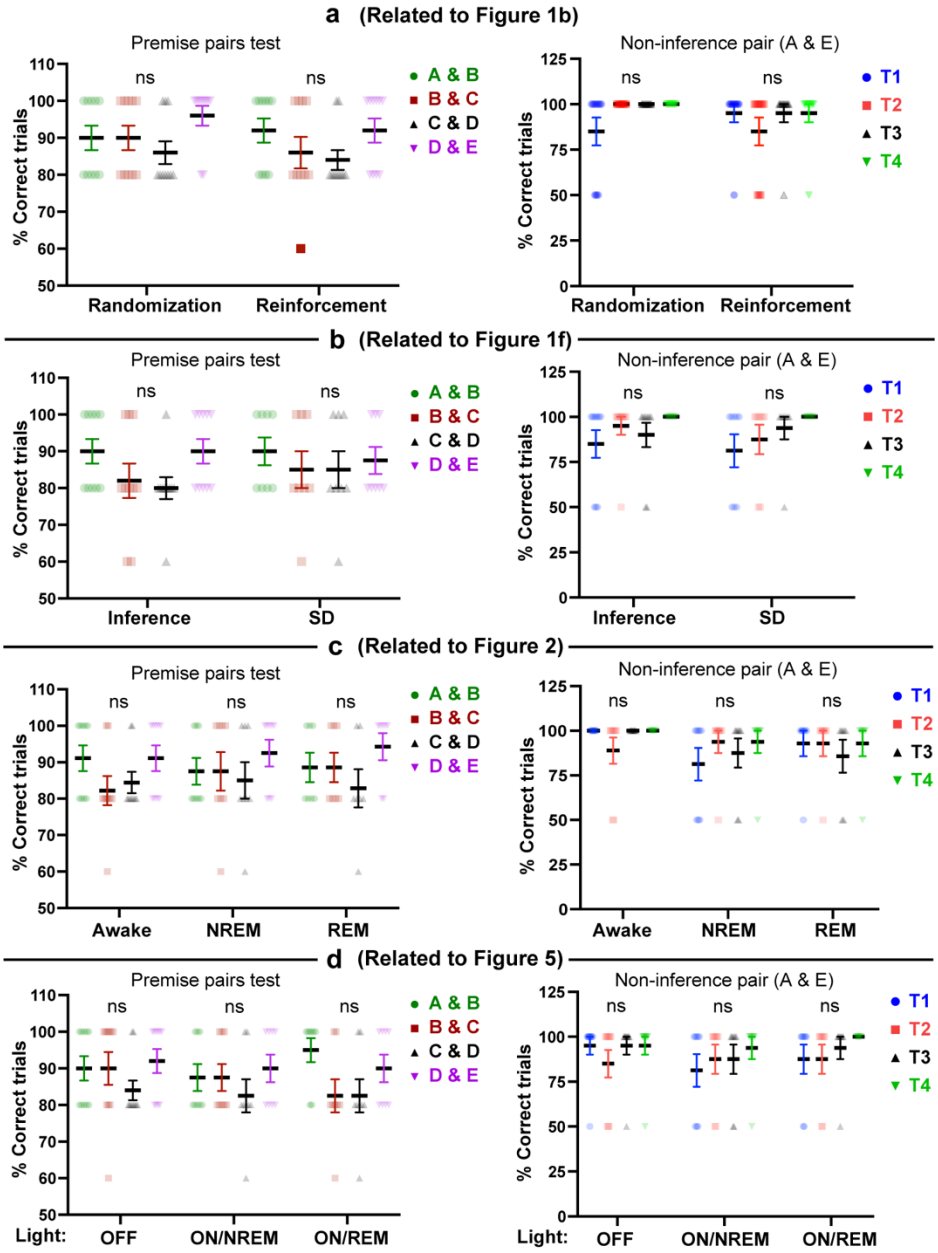

Extended Data Fig. 2 | Correct performance during testing original premise pairs and non-inference pair. a-d, Performance during test sessions; the percent of correct trials during the original premise pairs test (left) and during the non-inference test (right). T1, test 1; T2, test 2; T3, test 3; T4, test 4. SD, sleep deprivation; NREM, non-rapid eye movement; REM, rapid eye movement. The number of animals in each panel is mentioned in the corresponding Figure legend. Statistical comparisons were made using a two-way repeated-measures analysis of variance (ANOVA) with Tukey's multiple comparison test (**a-d**). ns, not significant ($P > 0.05$). Data are presented as the mean ± standard error of the mean (s.e.m.).

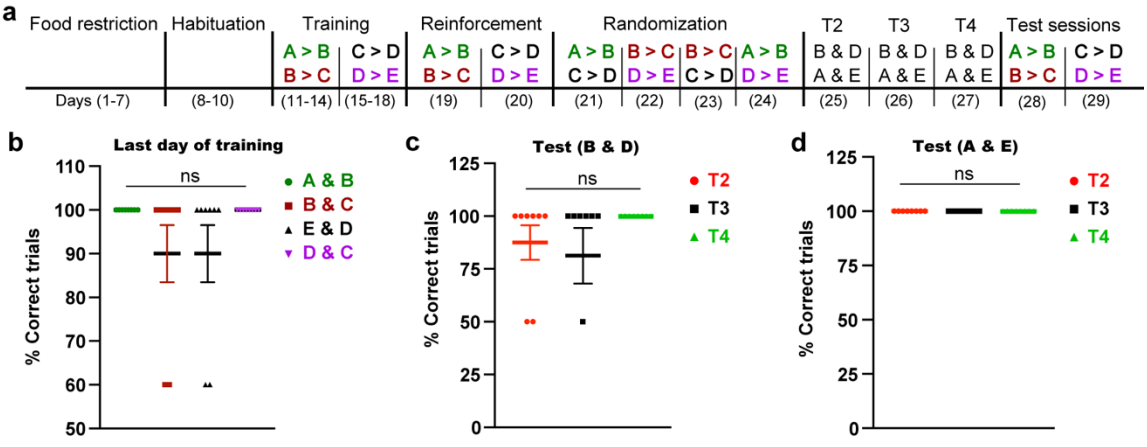

Extended Data Fig. 3 | Inferential behaviour does not require priming by preexposure to the testing environment. a, The behavioural schedule used to test the impact of the complete hierarchy on inference development. The order of presentation of the premise pairs during the randomization stage is different across animals within the same group (See Methods; Table 1). **b**, The performance during the last day of training (day 14 for A > B and B > C; day 18 for E > D and D > C) for each premise pair was calculated as the percent of correct trials out of the total number of trials. **c-d,** Performance during test sessions; the percent of correct trials during the inference test (**c**) and during the non-inference test (**d**). Statistical comparisons were made using a one-way repeated-measures analysis of variance (ANOVA) with Tukey's multiple comparison test; n=8 mice; ns, not significant ($P > 0.05$). Data are presented as the mean ± standard error of the mean (s.e.m.).

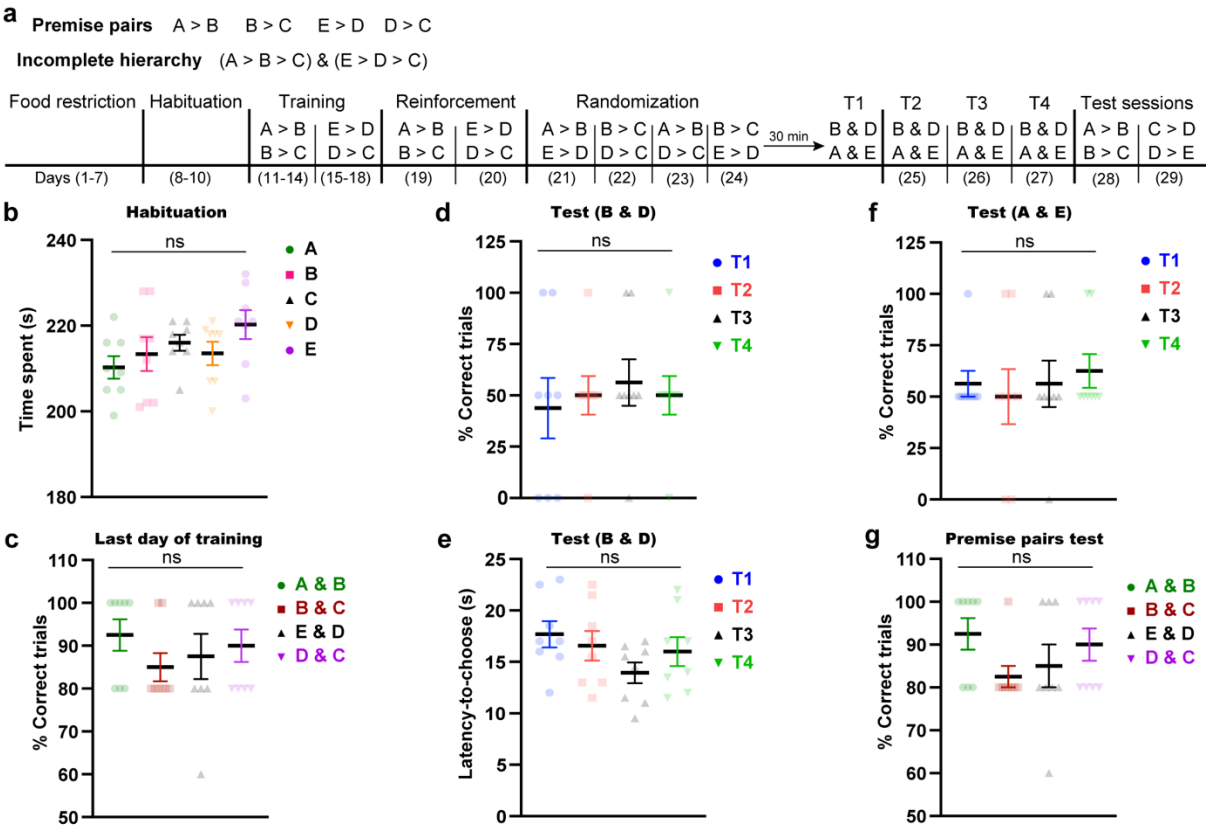

Extended Data Fig. 4 | Without the complete hierarchy, mice could not infer correctly. a, The behavioural schedule used to test the impact of the complete hierarchy on inference development. **b**, Time spent in each context during the habituation phase. **c,** The performance during the last day of training (day 14 for A > B and B > C; day 18 for E > D and D > C) for each premise pair was calculated as the percent of correct trials out of the total number of trials. **d-g,** Performance during test sessions; the percent of correct trials during the inference test (**d**), the latency time to choose during the inference test (**e**), during the non-inference test (**f**), during the original premise pairs test (**g**). T1, test 1; T2, test 2; T3, test 3; T4, test 4. n = 8 mice. Statistical comparisons were made using a one-way repeated-measures analysis of variance (ANOVA) with Tukey's multiple comparison test (**b-g**). ns, not significant ($P > 0.05$). Data are presented as the mean ± standard error of the mean (s.e.m.).

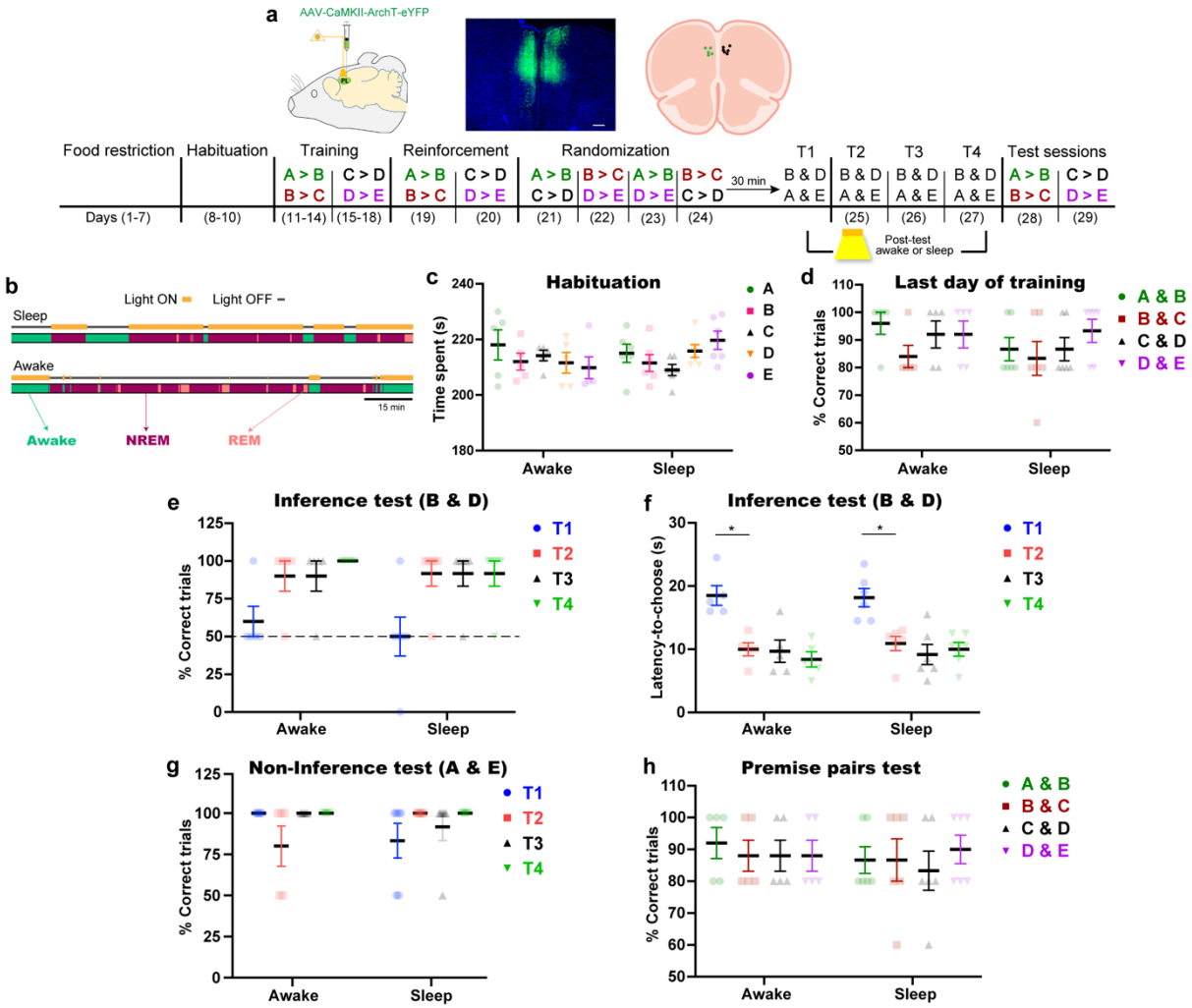

Extended Data Fig. 5 | Prelimbic cortex activity is not required for the emergence of inference. a, Top, Labelling of excitatory neurons of the prelimbic cortex (PL) with ArchT (left), coronal section from the mouse brain showing the expression of ArchT-eYFP (green) in the PL (middle) and optic fibre tip location (right). Black dots, mice in the awake group; Green dots, mice in the sleep group. Blue, 4′,6-diamidino-2-phenylindole (DAPI) staining. Scale bar, 100 µm. Bottom, The behavioural schedule used to manipulate PL activity during sleep or awake periods after test sessions. The order of presentation of the premise pairs during the randomization stage is different across animals within the same group (See Methods; Table 1). **b**, Diagram showing the state-specific manipulation. Scale bar, 15 minutes. **c,** Time spent in each context during the habituation phase**. d,** Performance during the last day of training (day 14 for A > B and B > C; day 18 for C > D and D > E) for each premise pair. **e-h,** Performance

during the test sessions; the percent of correct trials during the inference test (**e**), latency time to choose during the inference test (**f**), during the non-inference test (**g**), during the original premise pairs test (**h**). T1, test 1; T2, test 2; T3, test 3; T4, test 4. $n = 5$ mice for the awake group; $n = 6$ mice for the sleep group. Statistical comparisons were made using a two-way repeated-measures analysis of variance (ANOVA) with Tukey's multiple comparison test (**c-h**). In the non-inference test (**g**), the statistical significance denotes the comparison between performance of the two groups relative to the chance level (50%). *$P < 0.05$; ****$P < 0.0001$; ns, not significant ($P > 0.05$). Data are presented as the mean ± standard error of the mean (s.e.m.).

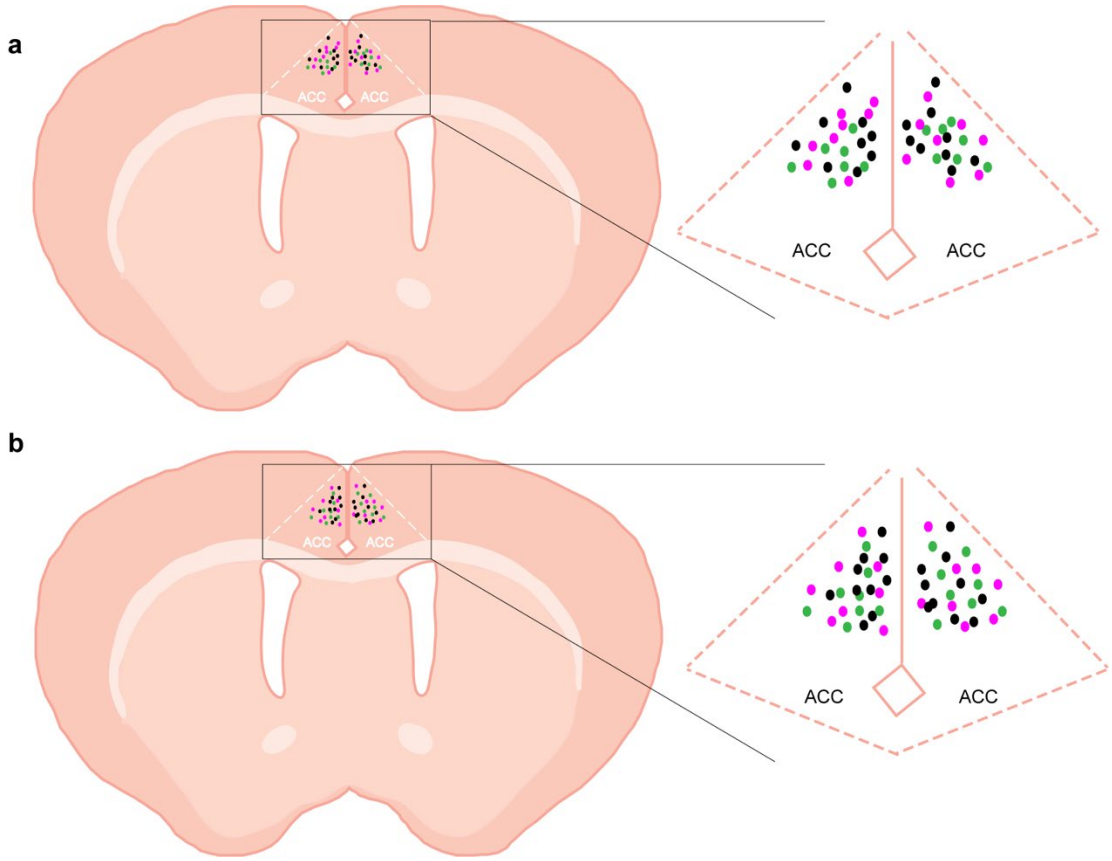

Extended Data Fig. 6 | Optic fibre locations in mice used in the manipulation experiments. **a**, Coronal section from the mouse brain showing the optic fibre tip location for mice shown in Fig. 2. Black dots, mice in the awake group; Green dots, mice in the NREM group; Pink dots, mice in the REM group. **b**, Coronal section from the mouse brain showing the optic fibre tip location for mice shown in Fig. 5. Black dots, mice in the light off group; Green dots, mice in the NREM group; Pink dots, mice in the REM group. The anterior cingulate cortex (ACC) is indicated by dashed lines.

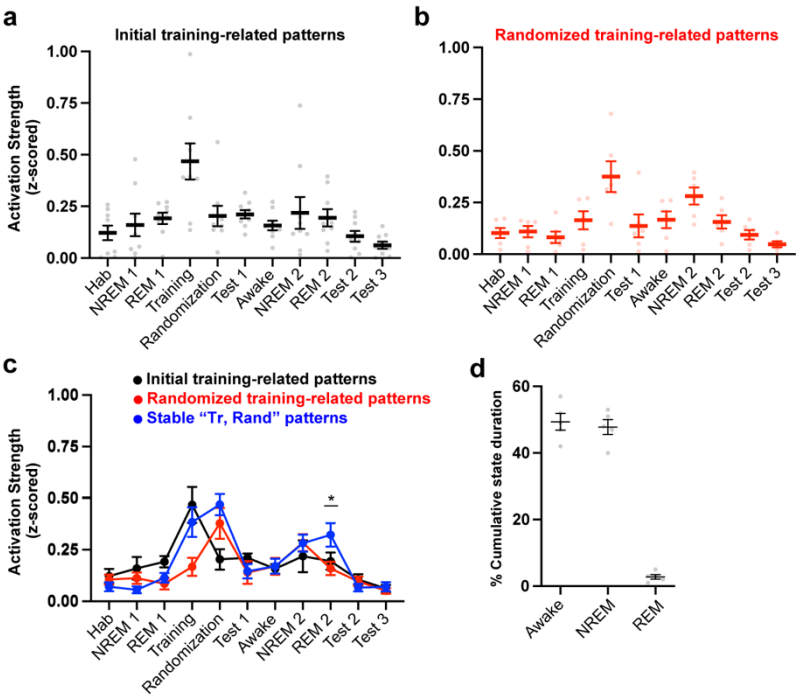

1054

1055 **Extended Data Fig. 7 | Temporally different patterns representing the original premise**

1056 **pairs. a-c**, Activation strength (z-scored) of the patterns representing the original premise pairs

1057 during initial training phase (**a, c**), during randomized training phase (**b, c**). **d,** Cumulative

1058 duration of each state (awake and sleep states) in all 5 mice. Statistical comparison was done

1059 using unpaired t-test; *P < 0.05. Data are presented as the mean ± standard error of the mean

1060 (s.e.m.).

1061

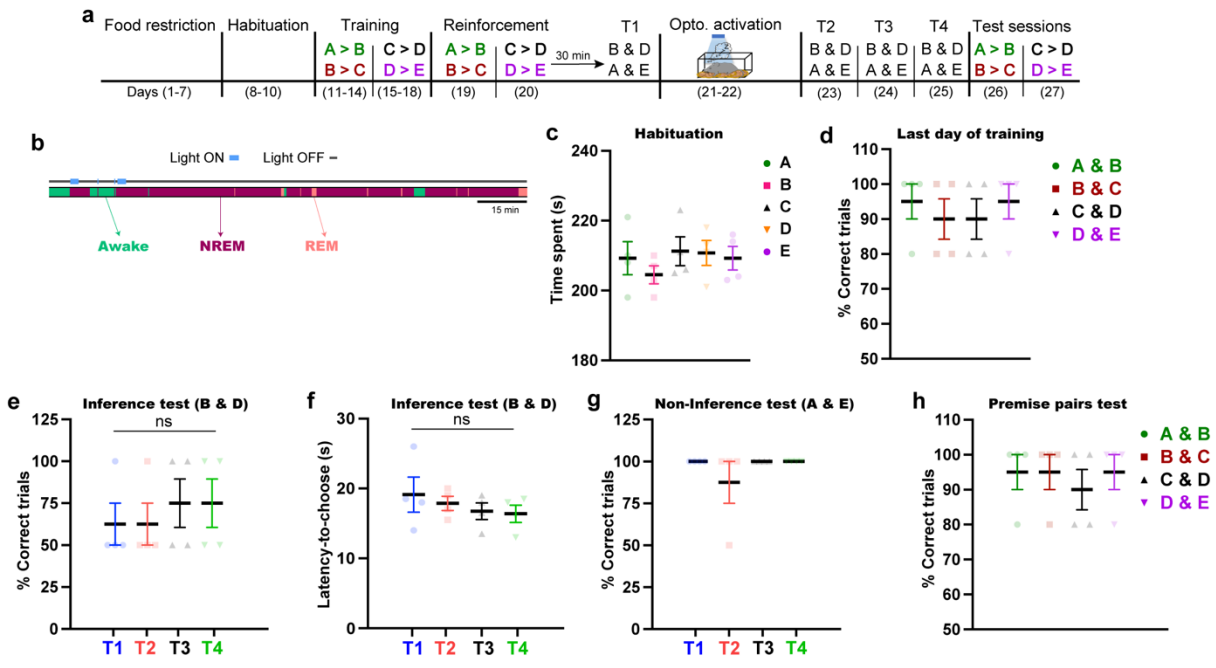

Extended Data Fig. 8 | Optogenetic activation of MEC→ACC circuit during NREM sleep is not sufficient for the emergence of inference. a, The behavioural schedule used to manipulate MEC→ACC circuit activity during NREM sleep after test sessions. **b**, Diagram showing the NREM-specific manipulation. The manipulation protocol mimicked the protocol used during REM sleep manipulation in Fig. 5 (see Methods) to avoid the prolonged light stimulation which might affect the results. Scale bar, 15 minutes. **c**, The time spent in each context during the habituation phase. **d**, Performance during the last day of training (day 14 for A > B and B > C; day 18 for C > D and D > E) for each premise pair. **e**-**h**, Performance during the test sessions; the percent of correct trials during the inference test (**e**), latency time to choose during the inference test (**f**), during the non-inference test (**g**), during the original premise pairs test (**h**). T1, test 1; T2, test 2; T3, test 3; T4, test 4; n = 4 mice. Statistical comparisons were made using a one-way repeated-measures analysis of variance (ANOVA) with Tukey's multiple comparison test (**c**-**h**). ns, not significant ($P > 0.05$). Data are presented as the mean ± standard error of the mean (s.e.m.).

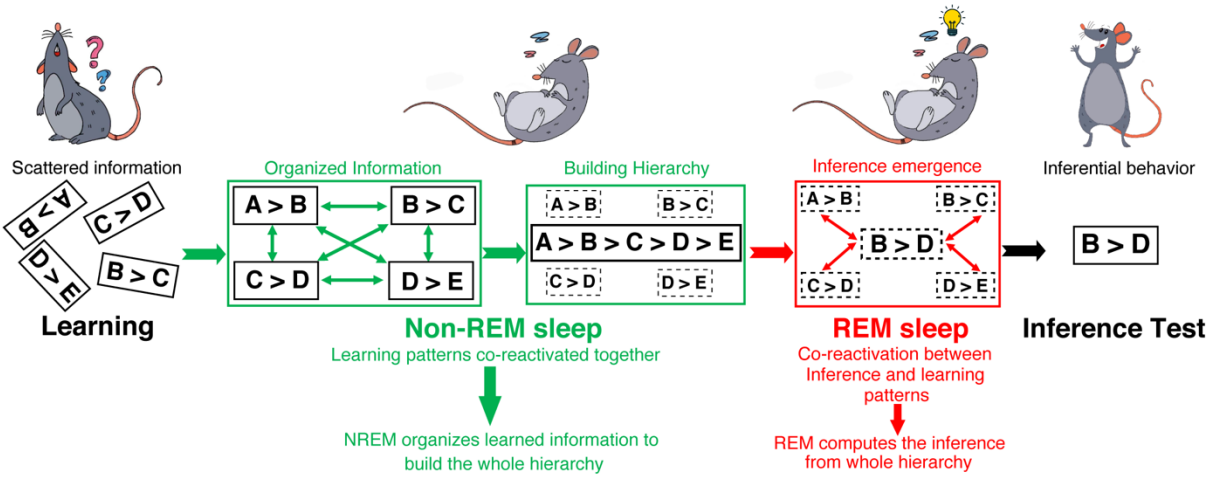

Extended Data Fig. 9 | A model of the coordinated roles of NREM & REM sleep in building inferential knowledge. Summary of the process of inference emergence. It starts with learning temporally distinct, but related information. Then, systematic organization of learned information in hierarchy during NREM sleep. Afterwards, building the inferential information from the hierarchy during REM sleep. Subsequently, inferential behaviour appears in the test session. An arrow with arrowheads at both ends indicates synchronous activity.